# Coordination between cytoskeletal organization, cell contraction and extracellular matrix development, is depended on LOX for aneurysm prevention

Rohtem Aviram[1], Shelly Zaffryar-Eilot[1], Anna Kaganovsky[1], Anas Odeh[1], Shay Melamed[1], Ruslana Militsin [4], Cameron B. Pinnock[2], Ariel Shemesh[5], Raz Palty[4], Santhi K. Ganesh[2,3] and Peleg Hasson[1,6]

[1] Department of Genetics and Developmental Biology, The Rappaport Faculty of Medicine and Research Institute, Technion – Israel Institute of Technology, Haifa, Israel.

[2] Frankel Cardiovascular Center, Division of Cardiovascular Medicine, Department of Internal Medicine, University of Michigan Medical School, Ann Arbor, MI, USA

[3] Department of Human Genetics, University of Michigan Medical School, Ann Arbor, MI, USA

[4] Department of Biochemistry, The Rappaport Faculty of Medicine and Research Institute, Technion – Israel Institute of Technology, Haifa, Israel.

[5] Biomedical core facilities, The Rappaport Faculty of Medicine and Research Institute, Technion – Israel Institute of Technology, Haifa, Israel.

[6] Corresponding author: phasson@technion.ac.il

Keywords: Lysyl oxidase, aneurysm, smooth muscle cell, cytoskeleton, extracellular matrix

**Abstract:**

Distinct, seemingly independent, cellular pathways affecting intracellular machineries or extracellular matrix (ECM) deposition and organization, have been implicated in aneurysm formation. One of the key genes associated with the pathology in both humans and mice is Lysyl oxidase (LOX), a secreted ECM-modifying enzyme, highly expressed in medial vascular smooth muscle cells. To dissect the mechanisms leading to aneurysm development, we conditionally deleted *Lox* in smooth muscle cells. We find that cytoskeletal organization is lost following *Lox* deletion. Cell culture assays and in vivo analyses demonstrate a cell-autonomous role for LOX affecting myosin light chain phosphorylation and cytoskeletal assembly resulting in irregular smooth muscle contraction. These results not only highlight new intracellular roles for LOX, but notably they link between multiple processes leading to aneurysm formation suggesting LOX coordinates ECM development, cytoskeletal organization and cell contraction required for media development and function.

36 **Introduction:**

37 Vascular smooth muscle cells (VSMCs) are the main cell type within the medial compartment of
38 large vessels such as the aorta. These VSMCs are the main source for the secretion of extracellular
39 matrix (ECM) and contraction, activities that are indispensable for vascular development,
40 maintenance and regulation of blood pressure. Disruption of these VSMC activities results in
41 thoracic aortic disease (TAD) manifesting in multiple vascular pathologies including aneurysms,
42 dissections and stenosis.

43 Three main groups of pathogenic genetic variants affecting VSMCs have been associated with TAD
44 [1]. These include ECM structural proteins (primarily those composing or regulating the
45 development of elastic fibers and collagens), members of the transforming growth factor β (TGFβ)
46 signaling pathway and genes involved in VSMC contractile machinery [2]. While an intimate link
47 between structural components of the ECM and TGFβ signaling has been previously
48 demonstrated [3], it is less clear why disruption of the VSMC contractile machinery results in
49 aneurysm formation in a similar manner to that observed in connective tissue (or ECM)
50 pathologies and what are the mechanisms that link between these causes.

51 LYSYL OXIDASE (LOX) is a key enzyme belonging to the lysyl oxidase family of secreted ECM
52 modifiers consisting of LOX and LOX-Like (LOXL) 1-4. LOX is highly expressed in VSMCs and is the
53 predominant family member in the aortic media [4,5]. LOX is secreted as a proenzyme and is cleaved
54 by various proteases. Following cleavage, both the mature active enzyme and its N-terminal
55 propeptide (LOX-PP) are released and mediate distinct functions. Previous work has
56 demonstrated that in VSMC both LOX-PP and the mature active enzyme can enter the cell and
57 exert various activities [6–9]. Key primary targets for LOX enzymatic activity within the media are
58 elastin and collagens where it functions as the main enzyme mediating their crosslinking.

59 Accordingly, mutations affecting LOX expression or enzymatic activity lead to disruption of ECM
60 integrity and are associated with aneurysms in both humans and mice [10–13]. Surprisingly, although
61 LOX is one of the most prominent genes linked with TAD, no direct genetic assessment of its role
62 specifically in VSMC has been carried out in vivo.

63 To dissect mechanisms that underlie aneurysm development and involvement of VSMC in the
64 process, we used a conditional knockout strategy to delete *Lox* using Cre lines expressed under
65 the *Myh11* promoter, a promoter specifically expressed in SMCs. Using this strategy and
66 knockdown assays in human aortic SMCs (HAOSMC) we find that LOX plays a key cell-autonomous
67 role in regulating VSMC cytoskeleton in an ECM-independent manner. Disruption of this latter
68 activity results in deregulation of SMC contraction in the aortic media. Our results highlight a
69 hitherto unappreciated role for LOX and suggest that apart from the observed ECM defects,
70 disruption of its intracellular activities lead to abnormal cytoskeletal organization, deregulated
71 contraction, and inability to respond to altered ECM. Surprisingly, we find the latter activities are
72 enzyme- and ECM-independent. Our results therefore highlight a missing link between the three
73 distinct gene groups associated with aneurysms, thus serving as a molecular paradigm for the
74 development of phenotypes that culminate in aneurysm.

75

76 **Results:**

77 *VSMC-specific Lox deletion leads to aneurysms*

78 To dissect the mechanisms promoting TAD that could result in aneurysms, we set to specifically
79 delete *Lox*, an ECM modifying enzyme highly associated with aneurysms, in VSMC using a
80 conditional knockout strategy. Towards that end, we crossed the *Myh11:Cre*$^{ERT2}$ deleter line [14] to
81 mice bearing a *Lox* conditional knockout allele (*Lox*$^{fl}$) [15]. Upon weaning, at the age of 3 weeks,

82 *Myh11:Cre$^{ERT2}$; Lox$^{fl/fl}$* mice (or *Lox$^{fl/fl}$* as controls) were IP injected with tamoxifen (100µl,
83 20mg/ml) for 5 consecutive days and then on once a month. Surprisingly, we find that even
84 though aortic Lox levels were significantly downregulated (~65-90% deletion) as monitored by a
85 western blot (WB) analysis (Supp. Fig.1A,B), no gross observable phenotypes were detected in the
86 aortas of the mutant mice, no changes to their blood pressure was noted, and their lifespan was,
87 similarly, not affected.

88 The surprising lack of visible phenotype following *Lox* deletion in the VSMC led us to test whether
89 such aortas lacking Lox activity in their media could withstand hypertension. Towards that end, at
90 the age of 3 months, osmotic pumps (alzet) infused with Angiotensin II (AngII; 10mg/kg/day) were
91 subcutaneously implanted for the duration of one month to increase blood pressure. Blood
92 pressure was monitored after 8 days and in all cases no differences between control (*Lox$^{fl/fl}$*) and
93 mutant (*Myh11:Cre$^{ERT2}$; Lox$^{fl/fl}$*) mice were observed (Fig. 1A) altogether demonstrating that the
94 loss of Lox from the VSMC did not affect their ability to respond to AngII and become
95 hypertensive. Following one month, at 4 months of age, mice were harvested and their aortas
96 dissected. WB analysis demonstrates AngII infusion did not affect the extent of Lox deletion (Fig.
97 1B). While among the AngII-treated control mice (n=9; *Lox$^{fl/fl}$*), only one displayed an aneurysm,
98 all mice with reduced medial Lox [of the genotypes *Myh11:Cre$^{ERT2}$; Lox$^{fl/fl}$* or *Myh11:Cre$^{ERT2}$; Lox$^{fl/\Delta}$*
99 (n=10)], displayed at least one aneurysm (Fig. 1C). Aneurysms were located throughout the aorta,
100 in the abdominal regions as well as in the thoracic and arch regions. Altogether, these results
101 demonstrate that Lox activity in the media is essential for the withstanding of hypertensive
102 conditions.

103 Histological examination of the aneurysms, regardless of their location, demonstrated that as
104 expected, elastic lamellae marked by Verhoeff-Van Gieson (VVG) staining were severely affected
105 highlighting multiple tears; Masson's Trichrome (MTC) staining revealed increased collagen

106 deposition and infiltration of immune cells to the diseased region (Fig. 1D). Interestingly, upon
107 monitoring non-aneurysmal regions, no significant differences were observed in media width,
108 average thickness of elastic lamella and number of breaks within them, although collagen
109 deposition was significantly increased in thoracic regions of the mutant aorta irrespective of
110 aneurysm location (Fig. 1D-H). These observations were surprising, since *Lox* was depleted
111 throughout the aortic media, raising the hypothesis that although its deletion affected the VSMC-
112 dependent ECM and elastin crosslinking, it may have resulted in additional, possibly ECM-
113 independent processes that contributed to the aneurysms.

**Figure 1. *Lox* knockout in VSMC promotes aneurysm formation.** Blood pressure measurements of control ($Lox^{fl/fl}$) prior to and following AngII treatment as well as of $Myh11{:}Cre^{ERT2};Lox^{fl/fl}$ mice (A). Western blot for Lox of control and $Myh11{:}Cre^{ERT2};Lox^{fl/fl}$ mouse aortas following AngII treatment (B). Aortas of control (left) or $Myh11{:}Cre^{ERT2}; Lox^{\Delta/fl}$(right) infused with AngII (C). Note aneurysms in $Myh11{:}Cre^{ERT2}; Lox^{\Delta/fl}$ (marked with *). Histological staining of *control* (left) and $Myh11{:}Cre^{ERT2};Lox^{fl/fl}$ (middle and right) aortic sections for Verhoeff Van-Gieson (VVG), Mason's Trichrome (MTC) and H&E. Note in control aortas, properly formed elastic fibers and defined tissue layers in contrast to the area of aneurysm in mutant mice, with torn elastic fibers and cell infiltration at point of rupture (middle column). In contrast, in non-aneurysmal areas of mutant aorta (right) no defect in media width (E), elastic lamella thickness (F) or nicks within (G) were observed. Collagen deposition was not affected in abdominal regions yet was upregulated in thoracic ones (H) in comparison to control.

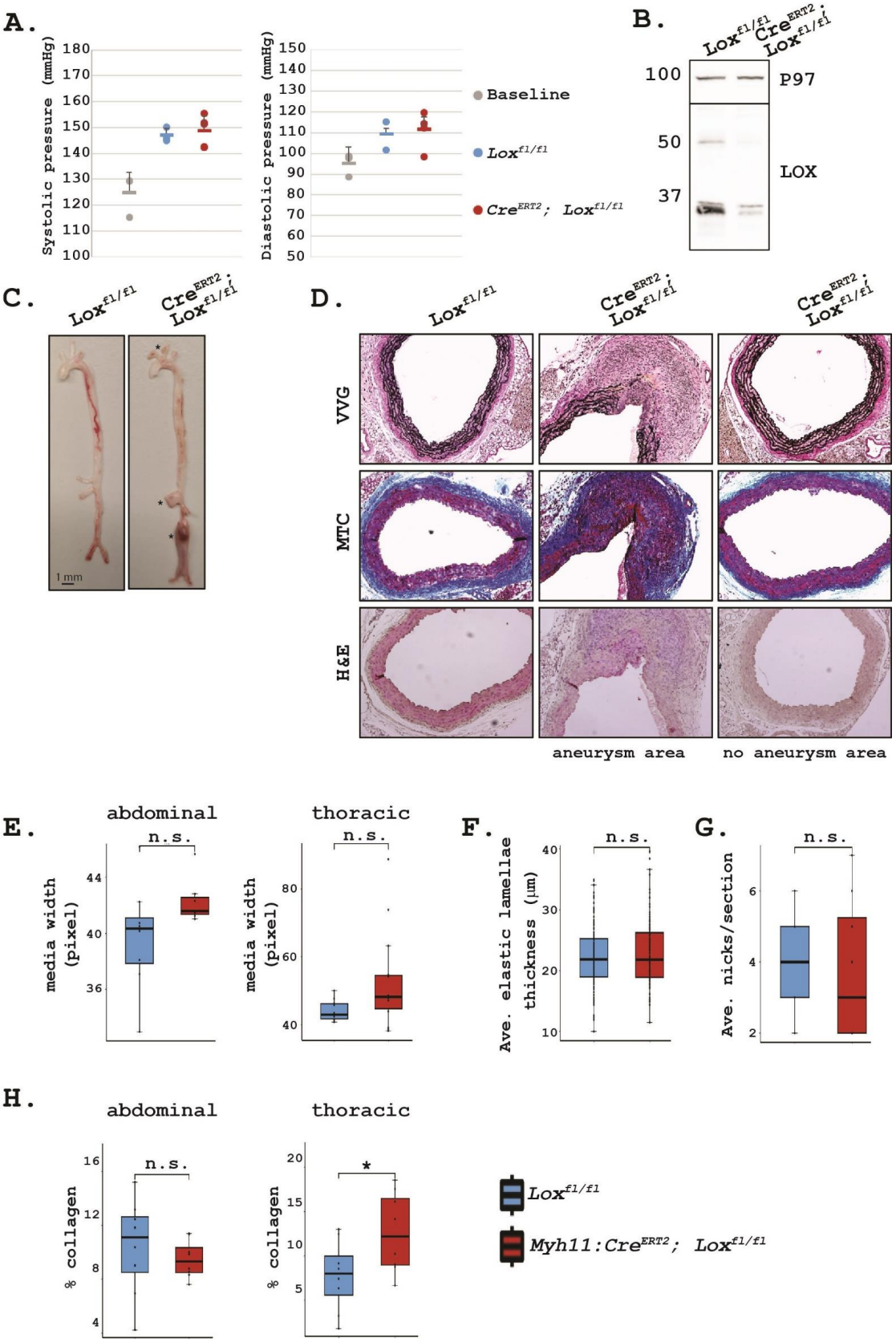
A.
Systolic pressure (mmHg)
Diastolic pressure (mmHg)
Baseline
Lox f1/f1
Cre ERT2; Lox f1/f1
B.
Lox f1/f1
Cre ERT2 Lox f1/f1
100
50
37
P97
LOX
C.
Lox f1/f1
Cre ERT2 Lox f1/f1
1 mm
D.
Lox f1/f1
Cre ERT2 Lox f1/f1
Cre ERT2 Lox f1/f1
VVG
MTC
H&E
aneurysm area
no aneurysm area
E.
abdominal
thoracic
n.s.
media width (pixel)
F.
Ave. elastic lamellae thickness (µm)
G.
Ave. nicks/section
H.
% collagen
*
Lox f1/f1
Myh11:Cre ERT2; Lox f1/f1

115 *LOX regulates multiple cellular behaviors*

116 To identify additional roles for Lox in VSMC, we took advantage of human aortic smooth muscle
117 cells (HAOSMC). These primary cells express high LOX levels and in a similar manner to that
118 observed in mice [4,5], it serves as the predominant family member in these cells (Fig. 2A). HAOSMC
119 secrete ECM [16] (see below) and can be easily manipulated in culture. To test if LOX levels can be
120 knocked-down we infected the cells with lentiviral particles expressing small hairpin sequences
121 targeting *LOX* (*shLOX*) or as control, a sequence with no target gene (*shCtrl*). We find that
122 following *LOX* knockdown, LOX protein levels were significantly downregulated without
123 considerably affecting the other members of the family (Fig. 2B,C). We also infected the cells with
124 two more *shLOX* lentiviral independent particles (marked as s*hLOX2* and *shLOX3*) where similar
125 inhibition of LOX expression was observed (Fig. 2C). Reduction in LOX expression via *shLOX*
126 resulted in a significant decrease in cell size (Fig. 2D-F). A comparable reduction in HAOSMC cell
127 size following *shLOX2* and *shLOX3* transfection was also observed (Fig. 2F). Thus, suggesting the
128 decrease in cell size phenotype was specific to *LOX* and not resulting from a non-specific target
129 inhibited by the small hairpin sequences.

130 The association of LOX with aneurysms has been suggested to be dependent on its enzymatic
131 activity where it regulates medial ECM formation and stabilization [5,10,12,17]. We therefore set to
132 test whether the observed HAOSMC phenotypes are likewise enzyme-dependent by adding
133 increasing concentrations of up to 500 µM of the pan-LOX inhibitor βAPN [18] or 10 µM of the LOX-
134 specific CCT365623 inhibitor [19]. Neither of these treatments affected LOX protein levels and
135 surprisingly they had no effect on HAOSMC cell size (Supp. Fig. 2A,B).

136 The lack of LOX enzymatic involvement raised the possibility that the observed phenotype might
137 be an activity associated with the LOX N-terminal region, LOX-PP, previously demonstrated to

138 inhibit VSMC proliferation [9]. However, in contrast to the phenotypes previously related to LOX-
139 PP, immunostaining for the proliferation associated marker Ki-67 demonstrated HAOSMC
140 depleted of LOX proliferated poorly (Supp. Fig. 2C,D). Live cell imaging over a 3-day period not
141 only reinforced the poor proliferation of the LOX-devoid cells, but also demonstrated they
142 exhibited increased cell death (Supp. Fig. 2E,F) altogether suggesting the observed phenotypes in
143 the *LOX* depleted cells are distinct from those associated with LOX-PP. Interestingly, while the
144 majority of nuclei in *shCtrl* cells appeared to be in a disc-like shape where only ~14% had an
145 irregular contour, 50% of the nuclei of *shLOX* cells were irregular (Supp. Fig. 2G,H). Overall, these
146 results suggest *LOX* depletion affected a general cellular property/properties independent of its
147 enzymatic activities.

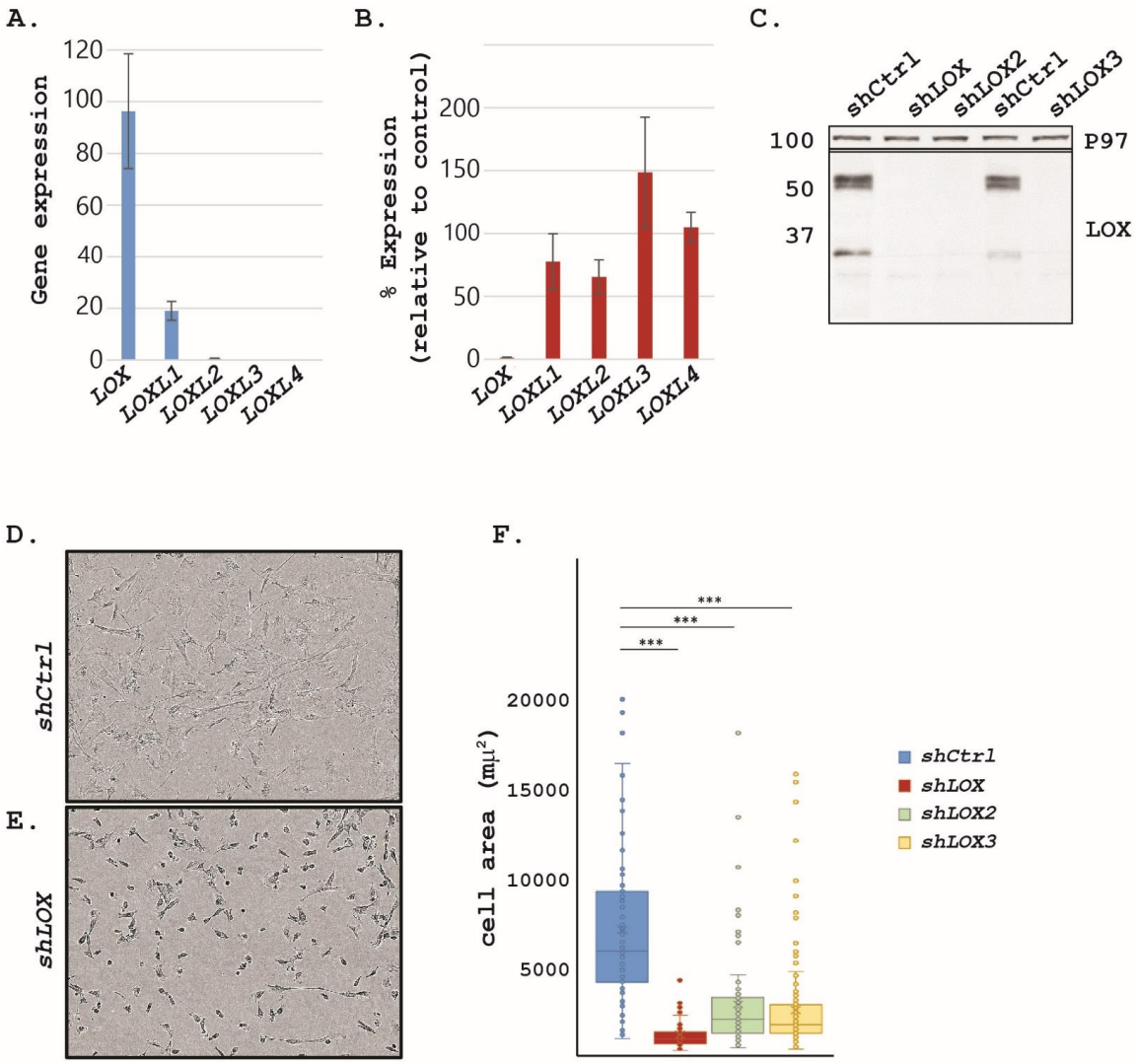


148

**Figure 2. *Lox* knockdown in HAOSMCs results in smaller cells.** Quantitative RT-PCR for *LOX* family members shows *LOX* is the predominant member of the family in HAOSMCs (A) Quantitative RT-PCR for *LOX* family members demonstrate they are not significantly affected by *LOX* deletion in HAOSMC (B). Western blot for LOX following knockdown with three distinct shRNA constructs demonstrate they all lead to significant LOX knockdown (C). Bright-field images of *shCtrl* (D) or *shLOX* (E) cells shows HAOSMCs devoid of *LOX* are smaller. Quantification of cell area reveals significant reduction in the 3 *shLOX* sequences (F).

149 *Autonomous LOX phenotypes*

150 LOX is a key ECM-modifier enzyme, hence we wished to test whether its depletion also affected
151 the ECM the cells secrete. Towards that end, we cultured the *shCtrl* and *shLOX* HAOSMC for 8
152 days, removed the cells, and the ECM they have secreted was then submitted to LC-MS/MS
153 analysis. As expected, significant differences were observed in ECM protein levels between the
154 control and LOX-depleted cells (Supp. Fig. 3A). Having seen these differences, we wished to test
155 whether the observed phenotypes could be attributed to the abnormal ECM secreted by the LOX-
156 depleted cells by assaying whether proper ECM could rescue them. Therefore, control HAOSMC
157 were cultured for 8-10 days and allowed to form a tight surface of compact cells and ECM (Supp.
158 Fig. 3B). Following culturing, cells were removed without affecting the ECM they have secreted
159 which remained bound to the tissue culture plates (Supp. Fig. 3C). *shCtrl* or *shLOX* HAOSMC were
160 then seeded directly onto the ECM (or onto standard tissue culture plates as control) and cultured
161 for 24 hours. Following plating *shCtrl* cells directly on plastic, the cells spread yet they do not
162 assume any directionality (Fig. 3A). In contrast, once they are plated onto mature ECM, they
163 rapidly elongate and assume the orientation of the ECM, i.e. that of the cells that have previously
164 laid it (Fig. 3B,C). In contrast, *shLOX* cells cultured on similarly mature ECM were comparable in
165 size and shape to those cultured directly on plastic (Fig. 3A,B). Further these LOX-devoid cells did
166 not elongate neither did they assume the orientation of the ECM they were laid upon (Fig. 3B,C).
167 Altogether, these results suggest the observed LOX-dependent phenotypes are not caused due to
168 an abnormal ECM laid by the mutant cells.

169 While LOX is mostly considered as a secreted enzyme where many of its activities are carried out
170 within the extracellular environment, previous work has suggested that cells, and primarily SMC,
171 can uptake exogenous mature enzyme [6]. We therefore reasoned that co-culturing LOX-depleted
172 cells with ones that secrete LOX, would rescue, at least to some extent, the observed phenotypes

173 (e.g., small cell size and reduced proliferation). Towards that end, GFP-transfected HAOSMC were
174 plated at a concentration of 1:1 and cultured with *shLOX* or *shCtrl* cells for one week. Cells were
175 imaged throughout this period. By the end of the week, the GFP-expressing HAOSMC cells
176 occupied ~50% of the dish when cultured with *shCtrl* cells suggesting they proliferated at similar
177 rates. In striking contrast, plates in which the *shLOX* and GFP-expressing HAOSMCs were co-
178 cultured, occupied primarily the GFP-expressing cells. These results demonstrate that although
179 the latter cells secreted LOX (Supp. Fig. 3D), the exogenous enzyme was not able to rescue the
180 proliferation or spreading of the *LOX*-depleted cells (Fig. 3D,E; Supp. Fig. 3E). To test whether the
181 reduced cell size of the *shLOX* cells was not caused by their inability to compete with the otherwise
182 wild-type GFP-expressing cells, we eliminated the latter GFP-marked cells as they did not express
183 any resistance marker. Following the addition of puromycin, only the *shCtrl* or *shLOX* cells which
184 stably express the knockdown construct survived. We find that following the removal of the GFP-
185 expressing cells, *shCtrl* cells spread, elongated and occupied the majority of the culture. In
186 contrast, the *shLOX* cells hardly proliferated and maintained their small size (Fig. 3F). Overall, the
187 combined results suggest the observed LOX-dependent phenotypes, which cannot be
188 compensated by exogenous LOX, are cell autonomous, and regulate the cells' ability to sense and
189 respond to distinct ECM environments.

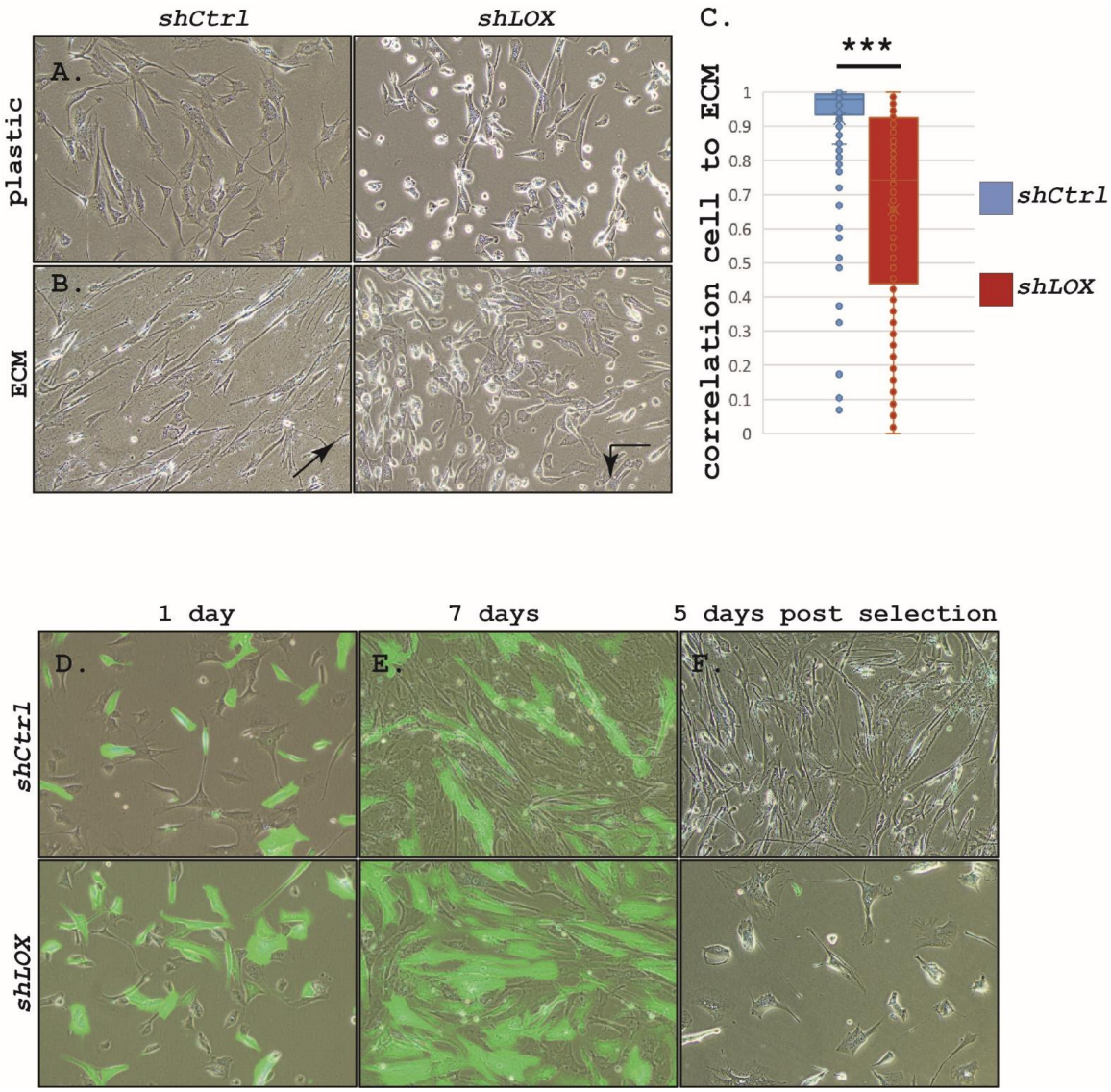


190

**Figure 3. LOX is autonomously required in HAOSMCs for interactions with the ECM.** *shCtrl* (left) or *shLOX* (right) cells cultured directly on plastic (A) or on HAOSMC-derived ECM (B). While *shCtrl* assume directionality of ECM they lay on (arrow in B, left), that of *shLOX* cells does not correlate to the ECM (arrow in B, right). Quantification of cell-to-matrix correlation shows significant differences between the cell genotypes (C). Bright-field and fluorescent images of GFP-tagged HAOSMCs co-cultured with *shCtrl* cells (D, top) or *shLOX* cells (D, bottom) and monitored for a week (E top and bottom, respectively). After 7 days the GFP cells were killed using puromycin selection leaving culture dishes with *shCtrl* (F, top) or *shLOX* (F, bottom) cells.

191 *LOX associates with cytoskeletal elements*

192 To test what could be the mechanism underlying the observed small cell size, defective nuclear
193 shape and the inability to respond to an ECM we set to identify LOX partners in the VSMC. We
194 immunoprecipitated LOX from HAOSMC cell lysates and submitted the precipitate to a LC-MS/MS
195 analysis (Supp. Table 1). Proteins identified by at least 3 distinct peptides, enriched at least 4 fold
196 with a p-value <0.05 in comparison to the control IgG precipitate were then submitted for
197 bioinformatics analysis. Kyoto Encyclopedia of Genes and Genomes (KEGG) analysis identified
198 significant enrichment of cytoskeleton-associated proteins to be precipitated with LOX (Supp. Fig.
199 4A). Monitoring cellular functions using Ingenuity Pathway Analysis (IPA) further reinforced the
200 significant enrichment of cytoskeletal elements among the proteins complexed, directly or
201 indirectly, with LOX (Supp. Fig. 4B).

202 The significant enrichment of cytoskeletal proteins associated with LOX containing complexes,
203 prompted us to monitor cytoskeletal arrangement in the *shLOX* HAOSMC. Staining for phalloidin
204 marking F-actin demonstrates significant disruption of actin organization. Although stress fibers
205 are present in the *shLOX* HAOSMC, many of the fibers are disrupted and do not extend the cells'
206 width or length as in the *shCtrl* HAOSMC (Fig. 4A). Immunostaining for tubulin reveals that in a
207 like manner to F-actin, the microtubule network was also disrupted and disorganized (Fig. 4B).
208 High-resolution transmission electron microscope (TEM) imaging further demonstrates that
209 cytoskeletal bundles are significantly disrupted in the *shLOX* cells (Fig. 4C).

210 To further dissect the disruption to the cytoskeleton, we monitored actin-binding proteins that
211 are abundant in VSMC. Smoothelin (SMTN), an actin binding protein aligns with the stress fibers
212 in control cells. However, following *LOX* knockdown this pattern is lost and SMTN is found
213 scattered within the cytoplasm (Fig. 5A). Notably, this disruption is not specific to SMTN;

214 monitoring other actin-binding proteins namely MyosinIIB, Calponin, SM22 (Transgelin; TAGLN)
215 and Filamin A, all revealed a similar pattern; while in the *shCtrl* cells these proteins aligned with
216 the stress fibers, in the *shLOX* cells, expression of these proteins was dispersed throughout the
217 cytoplasm and barely aligned with the fibers (Fig. 5B-E). Quantification of Smoothelin and SM22
218 expression demonstrated they were not significantly affected by the loss of LOX (Fig. 5F-H and LC-
219 MS/MS analysis, Supp. Table 2), indicating that cytoskeletal organization, rather the expression
220 levels of its components, are affected by the loss of LOX.

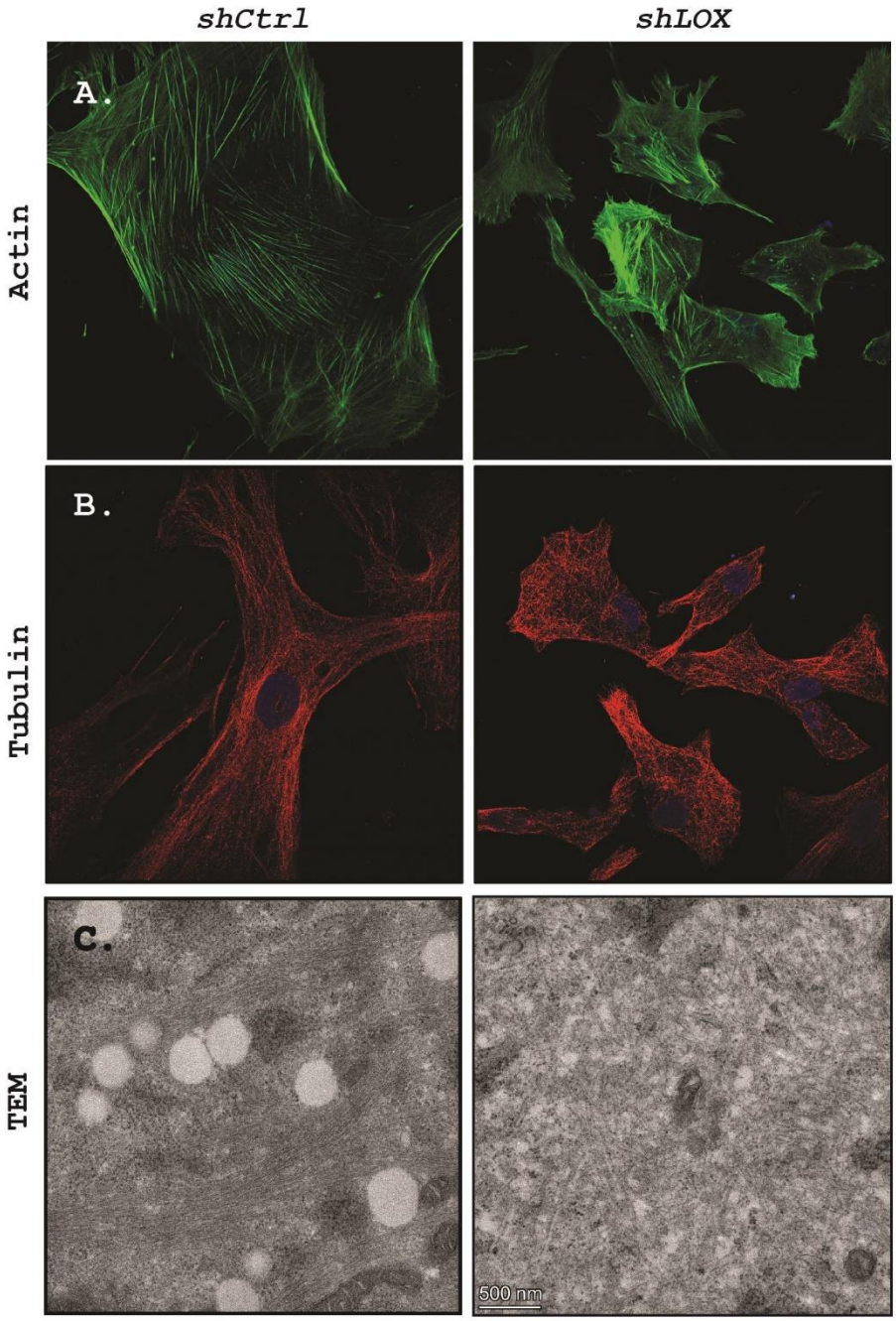


221

**Figure 4. *LOX* knockdown in HAOSMCs affects cytoskeletal organization.** Staining for actin (phalloidin, green; A) and tubulin (red; B) in *shCtrl* (left) and *shLOX* (right) HAOSMC. High magnification TEM images of *shCtrl* (left) and *shLOX* (right) shows cytoskeletal organization is significantly affected following *LOX* knockdown (C).

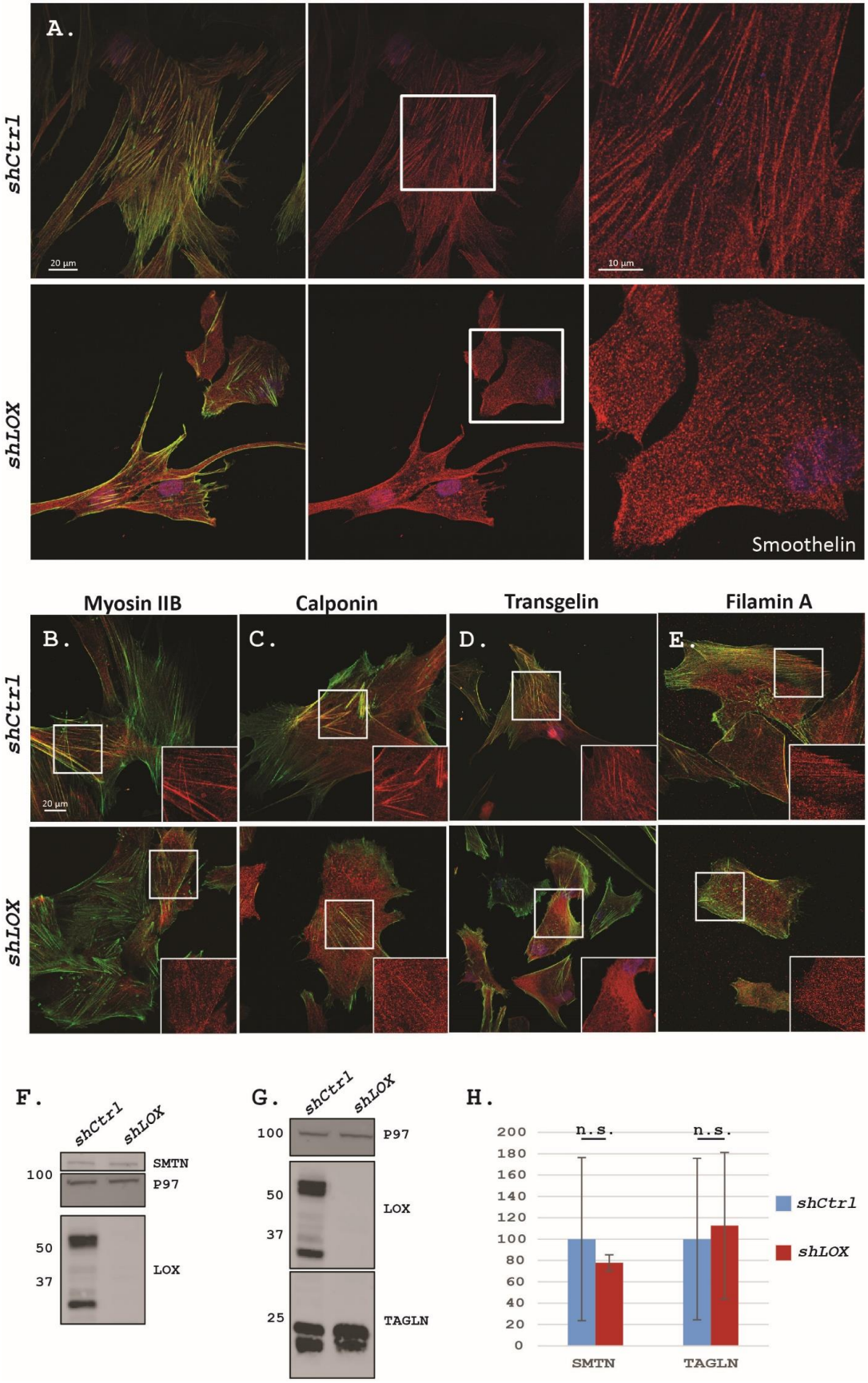
A.
shCtrl
shLOX
20 µm
10 µm
Smoothelin
Myosin IIB
Calponin
Transgelin
Filamin A
B.
C.
D.
E.
F.
shCtrl
shLOX
SMTN
P97
LOX
100
50
37
G.
P97
LOX
TAGLN
25
H.
n.s.
shCtrl
shLOX
SMTN
TAGLN
200
180
160
140
120
100
80
60
40
20
0

**Figure 5. Localization of actin binding proteins is disrupted following LOX knockdown.** Confocal images of *shCtrl* (A, top) and *shLOX* (A, bottom) HAOSMCs immunostained for for Smoothelin (red) and phalloidin (actin, green). Note Smoothelin localization to actin fibrils is lost in *shLOX* cells (higher magnification of boxed area in right panel). Confocal images of Myosin IIB (B), Calponin (C), Transgelin (D) and Filamin A (E) in *shCtrl* (top) and *shLOX* (bottom) HAOSMC shows similar disruption of actin binding proteins in cells devoid of LOX. Western blots for Smoothelin (F) and Transgelin (G) and corresponding quantification (H) in *shCtrl* and *shLOX* cells shows their levels are not affected following *LOX* knockdown.

223 *MLC phosphorylation is abnormally regulated in LOX mutant cells*

224 The small, gaunt appearance of the *shLOX* cells along with their abnormal cytoskeletal
225 organization raised the possibility that contraction of their actin cytoskeleton might be
226 abnormally regulated. The regulatory myosin light chain (MLC/Myl9) is the main regulatory
227 protein controlling actin contraction and phosphorylated MLC (p-MLC) is found on the
228 cytoskeletal contractile units. MLC is activated by phosphorylation that in turn is dually regulated
229 by a phosphatase (MLCP) and a kinase (MLCK)[20]. Deregulated MLC phosphorylation has been
230 associated with aneurysms and cardiovascular pathologies [20,21]. MLCP is inhibited by the Rho
231 associated kinases ROCK1 and ROCK2 hence these two kinases serve as positive regulators of
232 filamentous actin buildup. In addition, they have been shown to directly phosphorylate actin
233 binding proteins regulating their association with F-actin [22–24] altogether raising the hypothesis
234 they may be involved in the above phenotypes. LC-MS/MS analysis and WB of *shCtrl* and *shLOX*
235 HAOSMC demonstrated both these kinases are significantly down regulated in the latter (Supp.
236 Table 2; Fig. 6A,B). Culturing *shCtrl* and *shLOX* cells with a ROCK inhibitor mostly affected the *shCtrl*
237 cells but not the *shLOX* ones in agreement with the latter having an already reduced ROCK1/2
238 expression (Fig. 6C,D). As expected, ROCK inhibition in *shCtrl* cells significantly disrupted their F-
239 actin and in the filaments that were still present, no Smoothelin alignment was observed,
240 suggesting this is a ROCK-dependent process (Fig. 6D). Accordingly, the culturing of the cells with

241 a Rho activator II, also had little effect on the *shLOX* cells since ROCK proteins, the downstream

242 effectors of this activator, were not present for it to properly function (Fig. 6E).

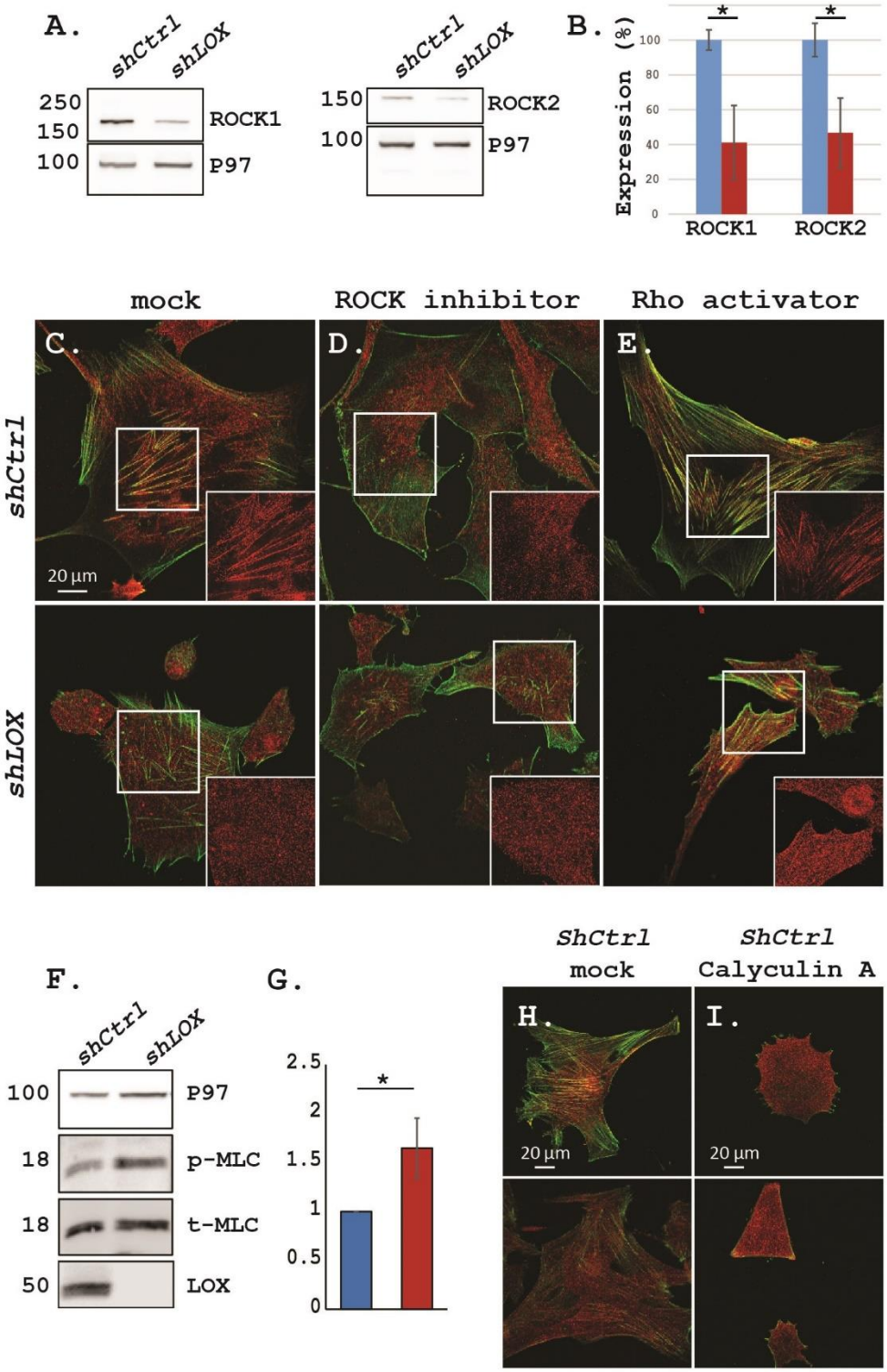


243

**Figure 6. *LOX* knockdown affects the Rho/ROCK pathway.** Western blot (A) and quantification (B) of ROCK1 and ROCK2 in *shCtrl* and *shLOX* HAOSMC shows ROCK proteins are downregulated following LOX deletion. Confocal images of immunostained HAOSMC for Smoothelin (red) and phalloidin (actin, green). Mock (C), ROCK inhibitor (D) or Rho activator (E) treated *shCtrl* (top) or *shLOX* (bottom) cells. Smoothelin localization to actin filaments is lost in *shCtrl* cells following ROCK inhibition (D) and is not regained following Rho activation in *shLOX* cells (E). WB (F) and quantification (G) of total and p-MLC in *control* and *shLOX* cells. Confocal images (2 images each, phaloidin green; Smoothelin, red) of untreated (H) and Calyculin A treated (I) *shCtrl* HOASMC demonstrate inhibition of MLC-phosphatase leads to reduced cell size and cytoskeletal defects.

244 The observation that the expression of the ROCK proteins was reduced in the LOX-devoid cells
245 suggested MLC activation, i.e. its phosphorylation, should be deregulated. WB for phosphorylated
246 MLC demonstrates upregulated phosphorylation (Fig. 6F,G). Culturing the *shCtrl* HAOSMC with
247 Calyculin A, a MLCP inhibitor, resulted in small *shLOX*-like cells with few organized F-actin
248 filaments (Fig. 6H,I) but also led to a significant increase in *shLOX* cell death (not shown).
249 Altogether, these results suggest that MLC activation is abnormally regulated in a ROCK/MLCP-
250 independent manner in the *LOX*-depleted cells.

251 We therefore set to test whether the other MLC regulator MLCK, a calcium-dependent kinase,
252 could be aberrantly regulated in the *shLOX* cells. MLCK is activated following calcium influx into
253 the cytoplasm from the cellular storages (e.g., sarcoplasmic reticulum) or from the extracellular
254 space, hence we monitored calcium homeostasis in the *LOX* knockdown and control cells.
255 Culturing the HAOSMC cells in calcium-free Ringer's solution and 0.2mM EGTA (a $Ca^{2+}$ chelator),
256 allowed us to monitor calcium cellular homeostasis in the *shCtrl* and *shLOX* cells. Using Fura-2 AM,
257 a fluorescent $Ca^{2+}$ indicator and ionomycin, a $Ca^{2+}$ ionophore that induces release of stored $Ca^{2+}$
258 to the cytoplasm, we traced the levels of cytosolic calcium before and after release of stored $Ca^{2+}$.
259 We find that *LOX* knockdown does not change resting $Ca^{2+}$ levels. However, while calcium levels
260 in cellular stores is also not affected (Fig. 7A), tracing the calcium levels demonstrates that the

261 ability of the *shLOX* cells to restore cytosolic calcium back to resting levels as monitored by the
262 rate of return to a steady state, is significantly inhibited (Fig. 7B-E). This finding suggest that
263 following a variety of physiologically relevant stimuli, *shLOX* treated cells would experience
264 prolonged periods of elevated cytosolic calcium and consequently abnormal MLCK activation.
265 Should MLCK activation be one of the causes of the observed phenotypes, we expect that its
266 inhibition will improve, at least to some extent, the *shLOX* phenotypes. Indeed, culturing the cells
267 (*shCtrl* or *shLOX* HAOSMC) for four days with a MLCK inhibitor resulted in a cell size increase and
268 the re-appearance of stress fibers in *shLOX* cells. In contrast, this treatment slightly worsened the
269 appearance of the control cells (Fig. 7F-H) altogether reinforcing the notion that MLCK is
270 abnormally regulated in the *shLOX* HAOSMC.

271

**Figure 7. LOX-deleted cells exhibit disrupted calcium homeostasis.** Intracellular calcium tracing show rate and magnitude of calcium release from intracellular storages and extracellular media are not altered in *LOX*-depleted cells (A). In contrast, the rate of calcium re-entry back into storages or its extracellular secretion is significantly inhibited in mutant cells (B). Single cell readings from *shCtrl* (C) and *shLOX* (D) as well as corresponding averages (E) demonstrate reduced rate of cytoplasmic calcium removal. Confocal images for phaloidin (green) and Smoothelin (red) of *shCtrl* cells with MLCK inhibitor results in minor defects of actin filament linearity (F, 2 images), whereas partially rescues *shLOX* cytoskeletal organization (G, 2 images) and leads to an increase in their cell size (H).

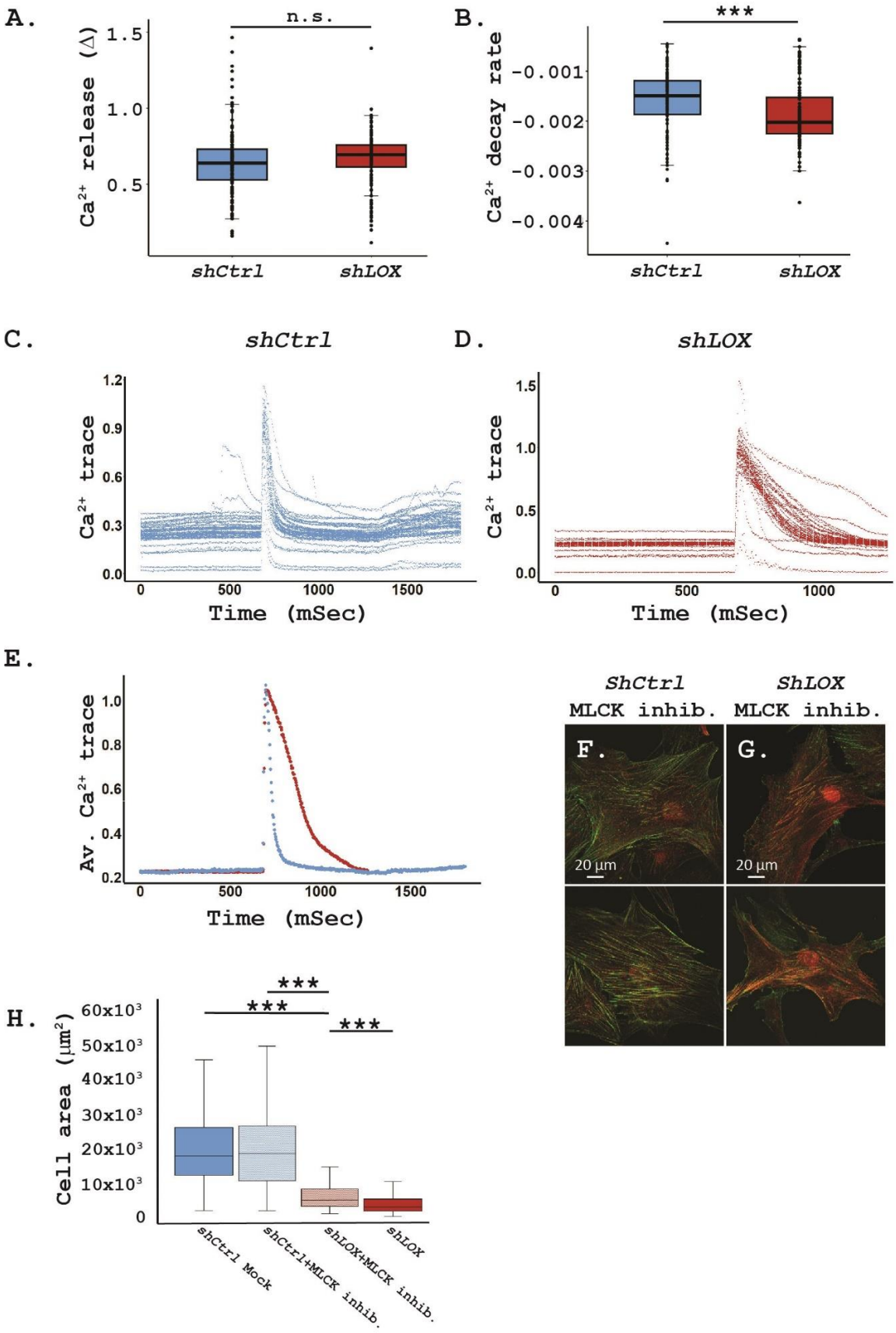
A.
n.s.
Ca2+ release (Δ)
1.5
1.0
0.5
shCtrl
shLOX
B.
***
Ca2+ decay rate
-0.001
-0.002
-0.003
-0.004
shCtrl
shLOX
C.
shCtrl
Ca2+ trace
1.2
0.9
0.6
0.3
0.0
0
500
1000
1500
Time (mSec)
D.
shLOX
Ca2+ trace
1.5
1.0
0.5
0.0
0
500
1000
Time (mSec)
E.
Av. Ca2+ trace
1.0
0.8
0.6
0.4
0.2
0
500
1000
1500
Time (mSec)
ShCtrl
MLCK inhib.
ShLOX
MLCK inhib.
F.
G.
20 µm
20 µm
H.
Cell area (µm2)
60x103
50x103
40x103
30x103
20x103
10x103
0
***
***
***
shCtrl Mock
shCtrl+MLCK inhib.
shLOX+MLCK inhib.
shLOX

272

273 The above observations were all carried out in cultured cells. Therefore, we next set to examine
274 whether these observations are relevant also to *Lox* roles in vivo in SMCs. We took advantage of
275 *Myh11:Cre*$^{EGFP}$ [25] which enables the deletion of a floxed gene in SMC from the onset of *Myh11*
276 expression without any requirement for Tamoxifen induction and monitored whether the
277 cytoskeleton is affected following this *Lox*-deletion regime. As with the Tamoxifen-induced Cre,
278 aneurysms were observed only following AngII infusion in *Myh11:Cre*$^{EGFP}$*; Lox*$^{fl/fl}$ mice (n=5, Supp.
279 Fig. 5) while non-hypertensive mice were viable, normally behaved and did not show any overall
280 phenotype demonstrating *Lox* deletion in SMC on its own even from early stages is not sufficient
281 for aneurysm formation. However, high resolution TEM imaging of medial SMCs demonstrated
282 cytoskeletal elements were significantly disorganized in the mutant aortas even without AngII-
283 mediated hypertension (Fig. 8A-C, higher magnification in A'-C'). Interestingly, upon monitoring
284 p-MLC immunostaining on aortic sections, we find that in control mice p-MLC immunostaining
285 intensities are rather uniform throughout the aortic media. In contrast, although absolute values
286 of p-MLC reach higher levels in *Myh11:Cre*$^{ERT2}$*; Lox*$^{fl/fl}$, immunostaining reveals a more variable
287 pattern of p-MLC expression (Fig. 8D-F). Spatial quantification of immunostaining intensities show
288 higher differences between the median and mean values in the mutant aortas (|median-
289 mean|=3.69 in control vs. 7.78 in mutant aortas; n=4 aortas of each genotype) (Fig. 8F)
290 demonstrating p-MLC inconsistent activation. Since p-MLC serves as a readout of cell contraction,
291 these observations suggest that SMC contraction in the *Lox* mutant aortas is scattered and
292 irregular.

293 Apart from regulating cell contraction, cytosolic $Ca^{2+}$ also regulates multiple other cellular
294 processes and its excessive levels are associated with increased mitochondrial deformities [26,27].
295 TEM imaging monitoring control and mutant aortas (n=4 mice of each genotype) demonstrate
296 that while in control mice ~4% of the mitochondria had a damaged appearance (n=93), in
297 *Myh11:Cre-EGFP; Lox*$^{fl/fl}$ >25% were damaged (n=182; Fig. 8A-C, black and pink arrows; Supp. Fig.
298 6). These results suggest that the observed scattered p-MLC activation might be due to reduced
299 mitochondrial activity stemming from the increased cytoplasmic $Ca^{2+}$.

**Figure 8. Lox regulates cytoskeletal organization in vivo independently of hypertension.** High resolution TEM images of aorta sections (A, control; B, C *Myh11:Cre*$^{EGFP}$*; Lox*$^{fl/fl}$ ) demonstrate lack of cytoskeletal organization in *Lox* knockout SMC even without hypertension. Black and pink arrows point to healthy and abnormal appearing mitochondria, respectively. Higher magnification of boxed areas A'-C'. Immunostaining for p-MLC (red) in control (D) and mutant (E) aortas demonstrates scattered and irregular cell activation. Histogram of p-MLC mean intensity frequency (n=4 of each genotype) demonstrate higher scattering of staining in *Myh11:Cre*$^{ERT2}$*; Lox*$^{fl/fl}$ mutant aortas than in the control (*Myh11:Cre*$^{ERT2}$) (F). Dotted lines indicate median values.

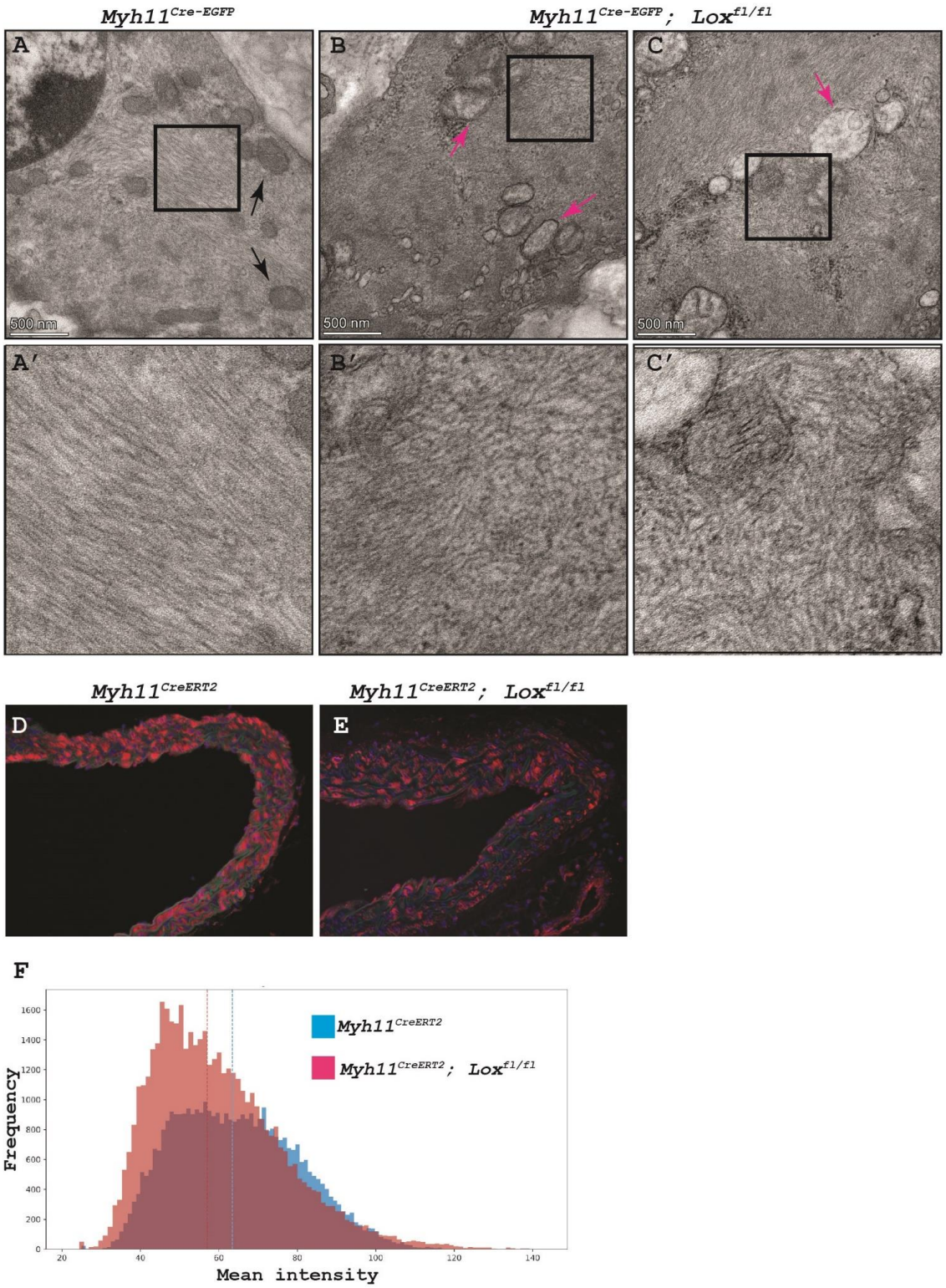
Myh11Cre-EGFP
Myh11Cre-EGFP; Loxfl/fl
A
B
C
500 nm
500 nm
500 nm
A′
B′
C′
Myh11CreERT2
Myh11CreERT2; Loxfl/fl
D
E
F
Frequency
Mean intensity
Myh11CreERT2
Myh11CreERT2; Loxfl/fl

300

301

302 **Discussion:**

303 Regulation of blood vessel integrity is key for maintaining proper vascular function. Disruption of
304 extracellular elements such as the elastic fibers were found to play a major role in the emergence
305 of weak spots, susceptible to rupture. Much work has focused on how cells within the media are
306 affected by defects in the ECM, however aberrant intracellular processes that can in turn affect
307 ECM and result in TAD have been given less attention. Administration of $\beta$APN leading to a pan
308 lysyl oxidase enzymatic inhibition, *LOX* mutations in humans and *Lox* knockout mice
309 demonstrated this enzyme, known for its role in elastin crosslinking, plays essential roles in the
310 vasculature and its inhibition or loss results in ECM defects that promote TAD [10,12,13]. Using a
311 conditional knockout strategy, we were able to directly examine Lox roles in VSMCs in vivo. By
312 focusing on the regions where no aneurysms occurred combined with cell culture assays, we
313 demonstrate that LOX plays an additional, as yet unappreciated, major intracellular role in
314 regulating VSMCs cytoskeleton affecting their contractile machinery.

315 Our finding that, intracellularly, LOX is highly enriched with cytoskeletal complexes along with the
316 significant cytoskeletal abnormalities observed following its loss prompted us to further explore
317 its involvement in the process. Phosphorylation of the myosin light chain serves as a key
318 regulatory event in the formation of the contractile units of actin cytoskeleton and as such is
319 tightly regulated via two main branches – ROCK1 and ROCK2 regulating MLC phosphatase on the
320 one hand and a calcium-dependent kinase on the other. Surprisingly, although we find that in
321 response to *LOX* knockdown ROCK1 and ROCK2 expression are significantly reduced, a process
322 which could lead to enhanced phosphatase activity, ectopic MLC phosphorylation was observed
323 raising the hypothesis that the calcium-dependent MLCK could be abnormally regulated. Probing
324 calcium homeostasis in *shLOX* cells demonstrated significant delays in the ability of these cells to
325 remove cytoplasmic calcium, suggesting it could underlie the observed prolonged MLCK activity

326 in HAOSMC devoid of LOX. However, in vivo, rather than an increase in MLC phosphorylation,
327 irregular and more scattered activation was observed. While this difference could be due to the
328 higher complexity in vivo with multiple feedback loops, our finding that mitochondrial damage
329 was more apparent in the *Lox*-mutant SMC could explain this observation.

330 Notably, hypertension induces vascular remodeling and SMC contraction [28], two processes which
331 also involve LOX. Previous reports have further implicated LOX as a regulator of TGFβ signaling [29–
332 31] but also as a downstream target for the pathway [32]. Since TGFβ signaling is implicated in
333 aneurysm formation [2,33] our observations, therefore, place LOX as a common player in the various
334 processes implicated in aneurysms.

335 Our results further suggest that not only are LOX activities spatially separated, but they also differ
336 in their dependence on its catalytic activities; while the intracellular regulation of cytoskeleton is
337 mediated via non-catalytic activities, extracellular ECM-crosslinking is enzyme-dependent.
338 Although LOX is an essential ECM-modifying enzyme, its intracellular roles are crucial for VSMC
339 viability and for the integrity of the aortic tissue. This work therefore suggest that in response to
340 reduced LOX expression, abnormal cytoskeletal organization leads to irregular smooth muscle cell
341 contraction and this, along with mild ECM defects, even in the lack of hypertension, predispose
342 the aorta to aneurysms. Thus, in agreement with previous findings where heterozygous *Lox* mice
343 were viable and did not show any or only a mild phenotype [5,10] it is plausible that the tissue
344 maintains its function for the most part even with low levels of Lox (~80% downregulation) and
345 that more critical phenotypes emerge with further reduction of its expression or induction of
346 hypertension. Altogether, linkage of both LOX extracellular and intracellular roles benefit our
347 understanding of arterial development and pathologies.

348

349 **Materials and Methods:**

350 **Mice.** All experiments involving mice conform to the relevant regulatory standards (AAALAC,
351 Technion IACUC and national animal welfare laws, guidelines and policies). All mice are housed in
352 IVC's (Techniplast) according to space requirements defined by the NRC. All rooms are set to have 22
353 °C ± 2° and humidity of 30–70%. All HVAC parameters are controlled by a central computerized
354 monitoring system. Light cycle is set to full light 10 h half-light 2 h and complete darkness 12 h, light
355 cycle is monitored by the computerized central system. *Lox*$^{fl}$ mice were previously described [15].
356 *SMMHC-CreER*$^{T2}$ (*MYH11:Cre*$^{ERT2}$) [14] and *smMHC*$^{Cre/eGFP}$ (*MYH11:Cre*$^{eGFP}$) [25] were purchased from JAX
357 mice (JAX strains 019079 and 007742, respectively). Cre activation for *SMMHC-CreER*$^{T2}$ mice was
358 carried out by injecting 50 µl tamoxifen (Sigma T5648, 20 mg/ml dissolved in corn oil) for 5
359 consecutive days to 3 week-old male mice, then 100 µl once a month. Hypertension induction was
360 carried out via subcutaneous implantation of osmotic pumps (Alzet mini-osmotic pump Model 2004;
361 0.25µl/hour, 28 days) loaded with Angiotensin II (AngII; 10mg/1kg/day) to 3 month-old mice.
362 Harvesting of aortas was performed 4 weeks after pump implantation.

363 **Cell Culture.** HAOSMCs were purchased and cultured according to the supplier's protocol (354-05A,
364 Sigma-Aldrich). Cells were further grown to passage 6, and used for experiments up to passage 11.
365 Smooth muscle cell growth media (311-500, Sigma-Aldrich) was used through all cell culturing. Kinase
366 modulation: HAOSMCs were cultured and infected with shRNA (*shLOX* and *shCtrl*). Cells were
367 trypsinized and seeded onto new dishes at 30% confluence. Two hours post seeding, the medium
368 was replaced with fresh growth medium containing either Calyculin A (Alomone labs C-100, 1nM),
369 MLCK inhibitor (Tocris 1885, 100 µM), Rho-Activator II (Cytoskeleton CN03, 2µg/ml), or ROCK
370 inhibitor y-s7632 (Peprotech 1293823, 1 µM). Cells were washed and fixed with 4%
371 paraformaldehyde after 24 hours (Rho-Activator, ROCK inhibitor), or 4 days (Calyculin A, MLCK
372 inhibitor).

373 **Lentiviral Infections.** HAOSMC infection, using viral particles generated in HEK293T cells, was carried
374 out according to standard protocols as previously described [34]. MISSION® shRNA lentiviral plasmids
375 (Merck) were used for knockdown of *LOX* (*shLOX1* – TRCN0000045991, *shLOX2* - TRCN0000293898,
376 *shLOX3* - TRCN0000286463) and a non-target shRNA was used for control (*shCtrl* – SHC016). Viral
377 particles generated by the HEK293T cells were collected in smooth muscle cell growth media, and
378 used to infect 1 million HAOSMC cells in a 10 cm dish. 24 hours post infection, the media was replaced
379 and Puromycin selection was administered for the following 5-7 days.
380 **Histochemistry.** Harvested mice aortas were fixed overnight in 4% paraformaldehyde, then
381 embedded in paraffin blocks. 3 µm sections were stained with Masson's Trichrome (MTC), Verhoeff's
382 Van Gieson (VVG), or Hematoxylin & Eosin.
383 **Immunohistochemistry.** Section immunohistochemistry were performed according to standard
384 protocols and as previously described [35]. The following antibodies were used: anti-Tubulin (abcam
385 ab4074, 1:300), anti-Smoothelin (ProteinTech 23567, 1:1000), anti-Transgelin (abcam ab14106,
386 1:1000), anti-Calponin (abcam ab46794, 1:500), anti-MyosinIIB (DSHB CMII23, 1:50), anti-Filamin A
387 (abcam ab76289, 1:200). Staining for F-actin was done using eGFP-conjugated phalloidin (Life
388 Technologies R37110, 1:1000).
389 **Western blot.** Protein lysates harvested from mice aortas or HAOSMCs were subjected to SDS-PAGE
390 analysis. Polyacrylamide gels were transferred to nitrocellulose membranes, which were then
391 probed with the following antibodies: anti-LOX (Cell Signaling D8F2K, 1:1000), anti-Smoothelin
392 (ProteinTech 23567, 1:1000), anti-Transgelin (abcam ab14106, 1:1000), anti-Calponin (abcam
393 ab46794, 1:5000), anti-ROCK1 (abcam ab97592, 1:1000), anti-ROCK2 (abcam ab125025, 1:3000),
394 anti-phospho-MLC2 (cell signaling 3674), and anti-MLC2 (cell signaling 3672). Loading was
395 determined using an anti-P97 (1:5000, kindly provided by Ariel Stanhill, Open University, IL).

396 **Immunoprecipitation.** Immunoprecipitations were done using 1 mg HAOSMC lysate, incubated with
397 2.5 µg anti-LOX (LS-C143168, LSBio) or IgG (011-000-003, Jackson Laboratories) as control, in a co-
398 immunoprecipitation buffer (20 mM Tris-HCl [pH 7], 150 mM NaCl, 2 mM EDTA, 1% NP-40) O/N at
399 4°C. Pre-clearing was done by incubating 2.5 µg IgG with the lysate prior to incubation with the
400 specific antibody. All antibodies were initially incubated with Dynabeads Protein G (1003D, Thermo
401 Fisher Scientific) in PBS [pH 7.4], 0.02% Tween-20 for 1 hour to form the conjugated complex of beads
402 with antibodies. After incubation with the lysate, protein complexes were washed three times in PBS
403 and subsequently extracted with SDS loading buffer for 3 minutes at 95°C. All incubations were
404 performed at 4°C with gentle rotation.
405 **RNA Isolation and cDNA Synthesis.** HAOSMC pellets were incubated with TRizol reagent (92608,
406 Ambion Life Technologies) to obtain cellular content. RNA was isolated using phase separation with
407 Chloroform. The RNA was then precipitated with isopropanol and washed with 75% EtOH. Following
408 RNA isolation, the RNA was reverse transcribed and cDNA was prepared using cDNA kit 5X All-In-One
409 RT MasterMix (abm G490) according to the manufacturer's instructions.
410 **Real-time Quantitative PCR.** Real-time qPCR was performed with the following probes from Sigma
411 Aldrich: LOX fw, CGGCGGAGGAAAACTGTCT; LOX rv, TCGGCTGGGTAAGAAATCTGA; LOXL1 fw,
412 CCACTACGACCTACTGGATGC; LOXL1 rv, GTTGCCGAAGTCACAGGTG; LOXL2 fw,
413 GGGTGGAGGTGTACTATGATGG; LOXL2 rv, CTTGCCGTAGGAGGAGCTG; LOXL3 fw,
414 TGGAGTTCTATCGTGCCAATGA; LOXL3 rv, CCTGAGGCTTCGACTGTTGT; LOXL4 fw,
415 CTGGGCACCACTAAGCTCC; LOXL4 rv, CTCCTGGATAGCAAAGTTGTCAT; GAPDH fw,
416 CATGAGAAGTATGACAACAGCCT; GAPDH rv, AGTCCTTCCACGATACCAAAGT.
417 Power SYBER Green PCR Master Mix (Thermo Fisher Scientific 4367659) was used for all reactions.
418 **Imaging.** Images were acquired using the Zeiss LSM 880 laser scanning confocal attached to Axio
419 Examiner Z1 upright microscope (Zeiss Germany), with X63 NA1.4 oil immersion objective and lasers

420 line 405nm, 488nm, 561nm, 633nm. The LSM 880 is controlled by ZEN Black 2.3 (Zeiss Germany).
421 Images used for nuclei analysis were acquire with Z stack. Quantitative image analysis of the nuclei
422 was performed by using Imaris software version 9.8.2 (Oxford Instruments, England). Each confocal
423 image was 3D reconstructed and segmented. HAOSMC live cell imaging of was acquired using the
424 Essen Bioscience Incucyte ZOOM, using X10 lens for 72 hours at 10 minute intervals.
425 **Transmission Electron Microscopy.** shRNA infected cells were grown on aclar film pretreated with
426 poly-L-lysine, washed and fixed for 1 hour with 2% Glutaraldehyde, 2% paraformaldehyde in 0.1 M
427 Sodium Cacodylate buffer (pH 7.4) containing 3% sucrose. The cells were washed with Cacodylate
428 buffer, post fixed for 30 min using 1% Osmium tetroxide in cacodylate buffer, washed with DDW and
429 incubated in 1% Uranyl Acetate for 30 min. Following dehydration in graded ethanol series, the aclar
430 films with cells were moved to fresh wells filled with Epon812 to start infiltration and embedding.
431 After polymerization, aclar film was pealed from the block and transverse sections were prepared.
432 For aorta imaging, the extracted tissue was cleaned, cut into ~2-3 mm thick rings, placed immediately
433 in the fixation solution containing 2% Glutaraldehyde, 2% paraformaldehyde in 0.1 M Sodium
434 Cacodylate buffer for 1 hour at RT and then moved to 4°c for 16 hours. The samples were washed,
435 post fixed with 1% Osmium Tetroxide for 1 hour, washed and en block stained with 2% Uranyl Acetate
436 for 60 min. Following dehydration using ethanol, the specimens were infiltrated with Epon812 for 3
437 days, oriented in silicon molds and after polymerization, crosswise sections were made.
438 Ultra-thin 75nm sections were cut using ultramicrotome UC7 (Leica), transferred to copper grids and
439 viewed using Talos L120C Transmission Electron Microscope at accelerating voltage of 120 kV.
440 **Mass Spectrometry Proteolysis:** from cell lysates- cell pellets were suspended in 9M Urea, 400mM
441 Ammonium bicarbonate and 10mM DTT following three cycles of sonication. 20ug protein from each
442 sample were reduced with 3mM DTT (60ºC for 30 min), modified with 9mM iodoacetamide in
443 100mM ammonium bicarbonate (in the dark, room temperature for 30 min) and digested in 1.5M

444 Urea, 66mM ammonium bicarbonate with modified trypsin (Promega) at a 1:50 enzyme-to-substrate
445 ratio, overnight at 37oC. An additional second trypsinization was done for 4 hours. For IP: Protein G
446 magnetic beads were suspended with 9M Urea, 400mM ABC, and incubated for 30' at room
447 temperature. Supernatant was transferred to a clean tube and reduced with 2.8mM DTT (60ºC for
448 30 min), modified with 8.8mM iodoacetamide in 100mM ammonium bicarbonate (in the dark, room
449 temperature for 30 min) and digested with Trypsin in 1.5M Urea, 66mM ammonium bicarbonate
450 with 0.1 µg of modified trypsin (Promega) overnight at 37oC.
451 **Mass spectrometry analysis:** The tryptic peptides were desalted using C18 tips (Top tip, Glygen) dried
452 and re-suspended in 0.1% Formic acid. Peptides were then resolved by reverse-phase
453 chromatography on 0.075 X 180-mm fused silica capillaries (J&W) packed with Reprosil reversed
454 phase material (Dr Maisch GmbH, Germany). Peptides were eluted with different concentrations of
455 Acetonitrile with 0.1% of formic acid: a linear 180 minutes gradient of 5 to 28% acetonitrile followed
456 by a 15 minutes gradient of 28 to 95% and 25 minutes at 95% acetonitrile with 0.1% formic acid in
457 water at flow rates of 0.15 µl/min. Mass spectrometry was performed by Q Executive HFX mass
458 spectrometer (Thermo) in a positive mode (m/z 300–1800, resolution 120,000 for MS1 and 15,000
459 for MS2) using repetitively full MS scan followed by collision induces dissociation (HCD, at 27
460 normalized collision energy) of the 30 most dominant ions (>1 charges) selected from the first MS
461 scan. The AGC settings were 3x106 for the full MS and 1x105 for the MS/MS scans. The intensity
462 threshold for triggering MS/MS analysis was 1x104. A dynamic exclusion list was enabled with
463 exclusion duration of 20 s. The mass spectrometry data was analyzed using the MaxQuant software
464 1.5.2.8 [36] for peak picking and identification using the Andromeda search engine, searching against
465 the human proteome from the Uniprot database with mass tolerance of 6 ppm for the precursor
466 masses and the fragment ions. Oxidation on methionine, Lysine and protein N-terminus acetylation
467 were accepted as variable modifications and carbamidomethyl on cysteine was accepted as static

468 modifications. Minimal peptide length was set to six amino acids and a maximum of two
469 miscleavages was allowed. Peptide- and protein-level false discovery rates (FDRs) were filtered to
470 1% using the target-decoy strategy. Protein table were filtered to eliminate the identifications from
471 the reverse database, and common contaminants and single peptide identifications. The data was
472 quantified by label free analysis using the same software.

473 **Cell to ECM correlation.** For brevity, cell to its surrounding ECM correlation was performed by
474 processing the cell and its matrix separately. The cells having large and distinguished shape were
475 segmented using a pre-trained convolutional neural network (CNN). In order to eliminate noise as
476 much as possible, small aggregates were also segmented and omitted from further steps in the
477 process.

478 The ECM was characterized with elongated but sometimes faint texture. Therefore, we commenced
479 by enhancing high frequencies using Embos filter, followed by random walker segmentation which
480 allows to strip out these fine structures. The ECM segmented structures were further refined
481 according to their aspect ratio. Principal component analysis (PCA) helped define the angle of each
482 piece of ECM. Using PCA, we similarly calculated the angle of cells, defining a new image of cells,
483 where their gray level values represented their angle. Then, an envelope that follows cell's outer
484 shape was defined, leaving the cell and some safety margins out of this envelope. This envelope
485 encompasses ECM structures, at which we calculated their median angle. At this point, we defined
486 another cells image, where the gray level of each cell was the angle of its surrounding ECM. At the
487 final stage, the correlation between cell's angle and the angle of its surrounding ECM was calculated
488 as the cosine of the angle difference between the cell and its surrounding ECM. Since both negative
489 and positive values have the same meaning, the absolute value was taken.

490 **Live-cell $Ca^{2+}$ imaging:** HAOSMCs were seeded on poly-L-Lysine (PLL, 5µg/ml) coverslips 1 day prior
491 to the experiment. Cells were loaded with 5µg/ml Fura-2 AM (Invitrogen), a fluorescent $Ca^{2+}$

492 indicator, in $Ca^{2+}$-free Ringer's solution for 30 min at room temperature. Next, the cells were washed
493 and transferred onto an imaging chamber and imaged using a fluorescence microscope. To
494 determine the plasma membrane Ca2+ ATPase (PMLC) activity, the cells were treated with Ca2+-free
495 Ringer's solution containing 2µM ionomycin (Alomone labs) and 0.2mM EGTA. The rate of Ca2+
496 clearance from the cytoplasm was determined by applying the exponential decay function in
497 R/Python software.

498 **p-MLC Image Analysis -** Python and its image processing libraries were used to analyze segmented
499 aortic images, focusing on quantifying red (p-MLC) regions. Using a (7, 7) kernel, we analyzed each
500 image segment for mean red intensity. Histograms were generated to visualize intensity
501 distributions, and the Kolmogorov-Smirnov test was used to compare the groups statistically.

502 **Mitochondrial Image Analysis and Segmentation -** We utilized Python along with Detectron2 to
503 conduct an in-depth analysis of images annotated for normal and abnormal mitochondria.
504 Annotations were carried out using MakeSense.

505

506 **Author Contribution**

507 R.A. conducted the majority of the experiments. S.Z.E. assisted in cell culture and western blot assays
508 and A.O., A.S. and S.M. assisted in image analysis. A.K. assisted in aorta isolations and western blot
509 analyses. R.K. and R.P. assisted in calcium-related assays. C.B.P. and S.K.G. assisted cell based assays
510 and data analyses. R.A. and P.H planned the study, supervised and analyzed the data.

511

512 **Acknowledgement**

513 The authors wish to thank the UM-Israel Partnership for Research to SKG and PH, Israeli Science
514 Foundation (1072/13) and (1111/18), by the Rappaport Family Foundation to P.H and NHLBI

515 R35HL161016 to SKG. We are grateful to M. Holdengreber from the BCF Bioimaging Center (Faculty
516 of Medicine, Technion); to Lihi Shaulov for TEM imaging; to members of the animal facility for
517 excellent technical assistance and to the Smoler Proteomics Center at the Technion.
518
519

520 **References**


521 1. Chou E, Pirruccello JP, Ellinor PT, Lindsay ME. Genetics and mechanisms of thoracic aortic
522 disease. *Nature Reviews Cardiology 2022* [Internet]. 2022 [cited 2022 Oct 11];1–13.
523 Available from: https://www.nature.com/articles/s41569-022-00763-0

524 2. Isselbacher EM, Lino Cardenas CL, Lindsay ME. Hereditary Influence in Thoracic Aortic
525 Aneurysm and Dissection. *Circulation*. 2016;133:2516–2528.

526 3. Benke K, Ágg B, Szilveszter B, Tarr F, Nagy ZB, Pólos M, Daróczi L, Merkely B, Szabolcs Z.
527 The role of transforming growth factor-beta in Marfan syndrome. *Cardiology journal*.
528 2013;20:227–234.

529 4. Mäki JM, Sormunen R, Lippo S, Kaarteenaho-Wiik R, Soininen R, Myllyharju J. Lysyl
530 oxidase is essential for normal development and function of the respiratory system and
531 for the integrity of elastic and collagen fibers in various tissues. *Am J Pathol* [Internet].
532 2005;167:927–936. Available from:
533 http://www.ncbi.nlm.nih.gov/entrez/query.fcgi?cmd=Retrieve&db=PubMed&dopt=Citati
534 on&list_uids=16192629

535 5. Lee VS, Halabi CM, Broekelmann TJ, Trackman PC, Stitziel NO, Mecham RP. Intracellular
536 retention of mutant lysyl oxidase leads to aortic dilation in response to increased
537 hemodynamic stress. *JCI Insight* [Internet]. 2019;5. Available from:
538 http://www.ncbi.nlm.nih.gov/pubmed/31211696

539 6. Nellaiappan K, Risitano A, Liu G, Nicklas G, Kagan HM. Fully processed lysyl oxidase
540 catalyst translocates from the extracellular space into nuclei of aortic smooth-muscle
541 cells. *Journal of cellular biochemistry*. 2000;79:576–582.

542 7. Li W, Nellaiappan K, Strassmaier T, Graham L, Thomas KM, Kagan HM. Localization and
543 activity of lysyl oxidase within nuclei of fibrogenic cells. *Proc Natl Acad Sci U S A*
544 [Internet]. 1997;94:12817–12822. Available from:
545 http://www.ncbi.nlm.nih.gov/entrez/query.fcgi?cmd=Retrieve&db=PubMed&dopt=Citati
546 on&list_uids=9371758

547 8. Kagan HM, Li W. Lysyl oxidase: properties, specificity, and biological roles inside and
548 outside of the cell. *J Cell Biochem* [Internet]. 2003;88:660–672. Available from:
549 http://www.ncbi.nlm.nih.gov/entrez/query.fcgi?cmd=Retrieve&db=PubMed&dopt=Citati
550 on&list_uids=12577300

551 9. Hurtado PA, Vora S, Sume SS, Yang D, St Hilaire C, Guo Y, Palamakumbura AH, Schreiber
552 BM, Ravid K, Trackman PC. Lysyl oxidase propeptide inhibits smooth muscle cell signaling
553 and proliferation. *Biochem Biophys Res Commun* [Internet]. 2008;366:156–161. Available
554 from: http://www.ncbi.nlm.nih.gov/pubmed/18060869

555 10. Mäki JM, Rasanen J, Tikkanen H, Sormunen R, Makikallio K, Kivirikko KI, Soininen R.
556 Inactivation of the lysyl oxidase gene Lox leads to aortic aneurysms, cardiovascular
557 dysfunction, and perinatal death in mice. *Circulation* [Internet]. 2002;106:2503–2509.
558 Available from:
559 http://www.ncbi.nlm.nih.gov/entrez/query.fcgi?cmd=Retrieve&db=PubMed&dopt=Citati
560 on&list_uids=12417550

561 11. Hornstra IK, Birge S, Starcher B, Bailey AJ, Mecham RP, Shapiro SD. Lysyl oxidase is
562 required for vascular and diaphragmatic development in mice. *J Biol Chem* [Internet].
563 2003;278:14387–14393. Available from:
564 http://www.ncbi.nlm.nih.gov/pubmed/12473682

565 12. Lee VS, Halabi CM, Hoffman EP, Carmichael N, Leshchiner I, Lian CG, Bierhals AJ, Vuzman
566 D, Mecham RP, Frank NY, Stitziel NO. Loss of function mutation in LOX causes thoracic
567 aortic aneurysm and dissection in humans. *Proc Natl Acad Sci U S A*. 2016;113:8759–
568 8764.

569 13. Guo DC, Regalado ES, Gong L, Duan X, Santos-Cortez RL, Arnaud P, Ren Z, Cai B, Hostetler
570 EM, Moran R, Liang D, Estrera A, Safi HJ, Leal SM, Bamshad MJ, Shendure J, Nickerson
571 DA, Jondeau G, Boileau C, Milewicz DM. LOX Mutations Predispose to Thoracic Aortic
572 Aneurysms and Dissections. *Circ Res*. 2016;118:928–934.

573 14. Wirth A, Benyo Z, Lukasova M, Leutgeb B, Wettschureck N, Gorbey S, Orsy P, Horvath B,
574 Maser-Gluth C, Greiner E, Lemmer B, Schuetz N, Gutkind S, Offermanns S. G(12)-G(13)-
575 LARG-mediated signaling in vascular smooth muscle is required for salt-induced
576 hypertension. *Nature Medicine*. 2008;14:64–68.

577 15. Gabay Yehezkely R, Zaffryar-Eilot S, Kaganovsky A, Fainshtain Malka N, Aviram R, Livneh I,
578 Hasson P. Intracellular role for the matrix modifying enzyme Lox in regulating
579 transcription factor subcellular localization and activity in muscle regeneration. *Dev Cell*.
580 2020;

581 16. Simmers P, Gishto A, Vyavahare N, Kothapalli CR. Nitric oxide stimulates matrix synthesis
582 and deposition by adult human aortic smooth muscle cells within three-dimensional
583 cocultures. *Tissue Engineering - Part A*. 2015;21:1455–1470.

584 17. Smith-Mungo LI, Kagan HM. Lysyl oxidase: properties, regulation and multiple functions
585 in biology. *Matrix Biol* [Internet]. 1998;16:387–398. Available from:
586 http://www.ncbi.nlm.nih.gov/pubmed/9524359

587 18. Narayanan AS, Siegel RC, Martin GR. On the inhibition of lysyl oxidase by -
588 aminopropionitrile. *Biochem Biophys Res Commun* [Internet]. 1972;46:745–751.
589 Available from:
590 http://www.ncbi.nlm.nih.gov/entrez/query.fcgi?cmd=Retrieve&db=PubMed&dopt=Citati
591 on&list_uids=5057904

592 19. Tang HR, Leung L, Saturno G, Viros A, Smith D, DI Leva G, Morrison E, Niculescu-Duvaz D,
593 Lopes F, Johnson L, Dhomen N, Springer C, Marais R. Lysyl oxidase drives tumour
594 progression by trapping EGF receptors at the cell surface. *Nature Communications*.
595 2017;8.

596 20. Ito M, Okamoto R, Ito H, Zhe Y, Dohi K. Regulation of myosin light-chain phosphorylation
597 and its roles in cardiovascular physiology and pathophysiology. *Hypertension research :*
598 *official journal of the Japanese Society of Hypertension*. 2022;45:40–52.

599 21. Milewicz DM, Trybus KM, Guo D-C, Sweeney HL, Regalado E, Kamm K, Stull JT. Altered
600 Smooth Muscle Cell Force Generation as a Driver of Thoracic Aortic Aneurysms and
601 Dissections. *Arteriosclerosis, thrombosis, and vascular biology*. 2017;37:26–34.

602 22. Amano M, Nakayama M, Kaibuchi K. Rho-kinase/ROCK: A key regulator of the
603 cytoskeleton and cell polarity. *Cytoskeleton (Hoboken, NJ)*. 2010;67:545–554.

604 23. Amano M, Ito M, Kimura K, Fukata Y, Chihara K, Nakano T, Matsuura Y, Kaibuchi K.
605 Phosphorylation and activation of myosin by Rho-associated kinase (Rho-kinase). *The*
606 *Journal of biological chemistry*. 1996;271:20246–20249.

607 24. Fukata Y, Amano M, Kaibuchi K. Rho-Rho-kinase pathway in smooth muscle contraction
608 and cytoskeletal reorganization of non-muscle cells. *Trends in pharmacological sciences*.

609 2001;22:32–39.

610 25. Xin H-B, Deng K-Y, Rishniw M, Ji G, Kotlikoff MI. Smooth muscle expression of Cre
611 recombinase and eGFP in transgenic mice. *Physiological genomics*. 2002;10:211–215.

612 26. Bernardi P, Rasola A. Calcium and cell death: the mitochondrial connection. *Sub-cellular*
613 *biochemistry*. 2007;45:481–506.

614 27. Smith MA, Schnellmann RG. Calpains, mitochondria, and apoptosis. *Cardiovascular*
615 *research*. 2012;96:32–37.

616 28. Lacolley P, Regnault V, Nicoletti A, Li Z, Michel JB. The vascular smooth muscle cell in
617 arterial pathology: a cell that can take on multiple roles. *Cardiovasc Res* [Internet].
618 2012;95:194–204. Available from: http://www.ncbi.nlm.nih.gov/pubmed/22467316

619 29. Kutchuk L, Laitala A, Soueid-Bomgarten S, Shentzer P, Rosendahl A-H, Eilot S, Grossman
620 M, Sagi I, Sormunen R, Myllyharju J, Mäki JM, Hasson P. Muscle composition is regulated
621 by a lox-TGFβ feedback loop. *Development (Cambridge)*. 2015;142.

622 30. Atsawasuwan P, Mochida Y, Katafuchi M, Kaku M, Fong KS, Csiszar K, Yamauchi M. Lysyl
623 oxidase binds transforming growth factor-beta and regulates its signaling via amine
624 oxidase activity. *J Biol Chem* [Internet]. 2008;283:34229–34240. Available from:
625 http://www.ncbi.nlm.nih.gov/entrez/query.fcgi?cmd=Retrieve&db=PubMed&dopt=Citati
626 on&list_uids=18835815

627 31. Grunwald H, Hunker KL, Birt I, Aviram R, Zaffryar-Eilot S, Ganesh SK, Hasson P. Lysyl
628 oxidase interactions with transforming growth factor-β during angiogenesis are mediated
629 by endothelin 1. *FASEB journal : official publication of the Federation of American*
630 *Societies for Experimental Biology* [Internet]. 2021 [cited 2022 Jul 4];35. Available from:

631 https://pubmed.ncbi.nlm.nih.gov/34370353/

632 32. Taylor MA, Amin JD, Kirschmann DA, Schiemann WP. Lysyl oxidase contributes to
633 mechanotransduction-mediated regulation of transforming growth factor-beta signaling
634 in breast cancer cells. *Neoplasia* [Internet]. 2011;13:406–418. Available from:
635 http://www.ncbi.nlm.nih.gov/pubmed/21532881

636 33. Jones JA, Spinale FG, Ikonomidis JS. Transforming growth factor-beta signaling in thoracic
637 aortic aneurysm development: a paradox in pathogenesis. *Journal of vascular research*
638 [Internet]. 2009 [cited 2022 Aug 6];46:119–137. Available from:
639 https://pubmed.ncbi.nlm.nih.gov/18765947/

640 34. Sengupta P, Seo AY, Pasolli HA, Song YE, Johnson MC, Lippincott-Schwartz J. A lipid-based
641 partitioning mechanism for selective incorporation of proteins into membranes of HIV
642 particles. *Nat Cell Biol*. 2019;21:452–461.

643 35. Hasson P, DeLaurier A, Bennett M, Grigorieva E, Naiche LA, Papaioannou VE, Mohun TJ,
644 Logan MPO. Tbx4 and Tbx5 Acting in Connective Tissue Are Required for Limb Muscle
645 and Tendon Patterning. *Developmental Cell*. 2010;18.

646 36. Cox J, Hein MY, Luber CA, Paron I, Nagaraj N, Mann M. Accurate proteome-wide label-
647 free quantification by delayed normalization and maximal peptide ratio extraction,
648 termed MaxLFQ. *Molecular & cellular proteomics : MCP* [Internet]. 2014 [cited 2022 Sep
649 1];13:2513–2526. Available from: https://pubmed.ncbi.nlm.nih.gov/24942700/

650

651

652 **Figure Legends**

653 **Figure 1. *Lox* knockout in VSMC promotes aneurysm formation.** Blood pressure measurements
654 of control ($Lox^{fl/fl}$) prior to and following AngII treatment as well as of $Myh11{:}Cre^{ERT2}{;}Lox^{fl/fl}$ mice
655 (A). Western blot for Lox of control and $Myh11{:}Cre^{ERT2}{;}Lox^{fl/fl}$ mouse aortas following AngII
656 treatment (B). Aortas of control (left) or $Myh11{:}Cre^{ERT2}{;}\ Lox^{\Delta/fl}$(right) infused with AngII (C). Note
657 aneurysms in $Myh11{:}Cre^{ERT2}{;}\ Lox^{\Delta/fl}$ (marked with *). Histological staining of *control* (left) and
658 $Myh11{:}Cre^{ERT2}{;}Lox^{fl/fl}$ (middle and right) aortic sections for Verhoeff Van-Gieson (VVG), Mason's
659 Trichrome (MTC) and H&E. Note in control aortas, properly formed elastic fibers and defined
660 tissue layers in contrast to the area of aneurysm in mutant mice, with torn elastic fibers and cell
661 infiltration at point of rupture (middle column). In contrast, in non-aneurysmal areas of mutant
662 aorta (right) no defect in media width (E), elastic lamella thickness (F) or nicks within (G) were
663 observed. Collagen deposition was not affected in abdominal regions yet was upregulated in
664 thoracic ones (H) in comparison to control.

665 **Figure 2. *Lox* knockdown in HAOSMCs results in smaller cells.** Quantitative RT-PCR for *LOX* family
666 members shows *LOX* is the predominant member of the family in HAOSMCs (A) Quantitative RT-
667 PCR for *LOX* family members demonstrate they are not significantly affected by *LOX* deletion in
668 HAOSMC (B). Western blot for LOX following knockdown with three distinct shRNA constructs
669 demonstrate they all lead to significant LOX knockdown (C). Bright-field images of *shCtrl* (D) or
670 *shLOX* (E) cells shows HAOSMCs devoid of *LOX* are smaller. Quantification of cell area reveals
671 significant reduction in the 3 *shLOX* sequences (F).

672 **Figure 3. LOX is autonomously required in HAOSMCs for interactions with the ECM.** *shCtrl* (left)
673 or *shLOX* (right) cells cultured directly on plastic (A) or on HAOSMC-derived ECM (B). While *shCtrl*
674 assume directionality of ECM they lay on (arrow in B, left), that of *shLOX* cells does not correlate

675 to the ECM (arrow in B, right). Quantification of cell-to-matrix correlation shows significant
676 differences between the cell genotypes (C). Bright-field and fluorescent images of GFP-tagged
677 HAOSMCs co-cultured with *shCtrl* cells (D, top) or *shLOX* cells (D, bottom) and monitored for a
678 week (E top and bottom, respectively). After 7 days the GFP cells were killed using puromycin
679 selection leaving culture dishes with *shCtrl* (F, top) or *shLOX* (F, bottom) cells.

680 **Figure 4. *LOX* knockdown in HAOSMCs affects cytoskeletal organization.** Staining for actin
681 (phalloidin, green; A) and tubulin (red; B) in *shCtrl* (left) and *shLOX* (right) HAOSMC. High
682 magnification TEM images of *shCtrl* (left) and *shLOX* (right) shows cytoskeletal organization is
683 significantly affected following *LOX* knockdown (C).

684 **Figure 5. Localization of actin binding proteins is disrupted following LOX knockdown.** Confocal
685 images of *shCtrl* (A, top) and *shLOX* (A, bottom) HAOSMCs immunostained for for Smoothelin (red)
686 and phalloidin (actin, green). Note Smoothelin localization to actin fibrils is lost in *shLOX* cells
687 (higher magnification of boxed area in right panel). Confocal images of Myosin IIB (B), Calponin
688 (C), Transgelin (D) and Filamin A (E) in *shCtrl* (top) and *shLOX* (bottom) HAOSMC shows similar
689 disruption of actin binding proteins in cells devoid of LOX. Western blots for Smoothelin (F) and
690 Transgelin (G) and corresponding quantification (H) in *shCtrl* and *shLOX* cells shows their levels
691 are not affected following *LOX* knockdown.

692 **Figure 6. *LOX* knockdown affects the Rho/ROCK pathway.** Western blot (A) and quantification
693 (B) of ROCK1 and ROCK2 in *shCtrl* and *shLOX* HAOSMC shows ROCK proteins are downregulated
694 following LOX deletion. Confocal images of immunostained HAOSMC for Smoothelin (red) and
695 phalloidin (actin, green). Mock (C), ROCK inhibitor (D) or Rho activator (E) treated *shCtrl* (top) or
696 *shLOX* (bottom) cells. Smoothelin localization to actin filaments is lost in *shCtrl* cells following
697 ROCK inhibition (D) and is not regained following Rho activation in *shLOX* cells (E). WB (F) and

698 quantification (G) of total and p-MLC in *control* and *shLOX* cells. Confocal images (2 images each,
699 phaloidin green; Smoothelin, red) of untreated (H) and Calyculin A treated (I) *shCtrl* HOASMC
700 demonstrate inhibition of MLC-phosphatase leads to reduced cell size and cytoskeletal defects.

701 **Figure 7. LOX-deleted cells exhibit disrupted calcium homeostasis.** Intracellular calcium tracing
702 show rate and magnitude of calcium release from intracellular storages and extracellular media
703 are not altered in *LOX*-depleted cells (A). In contrast, the rate of calcium re-entry back into
704 storages or its extracellular secretion is significantly inhibited in mutant cells (B). Single cell
705 readings from *shCtrl* (C) and *shLOX* (D) as well as corresponding averages (E) demonstrate reduced
706 rate of cytoplasmic calcium removal. Confocal images for phaloidin (green) and Smoothelin (red)
707 of *shCtrl* cells with MLCK inhibitor results in minor defects of actin filament linearity (F, 2 images),
708 whereas partially rescues *shLOX* cytoskeletal organization (G, 2 images) and leads to an increase
709 in their cell size (H).

710 **Figure 8. Lox regulates cytoskeletal organization in vivo independently of hypertension.** High
711 resolution TEM images of aorta sections (A, control; B, C *Myh11:Cre*$^{EGFP}$*; Lox*$^{fl/fl}$ ) demonstrate lack
712 of cytoskeletal organization in *Lox* knockout SMC even without hypertension. Black and pink
713 arrows point to healthy and abnormal appearing mitochondria, respectively. Higher magnification
714 of boxed areas A'-C'. Immunostaining for p-MLC (red) in control (D) and mutant (E) aortas
715 demonstrates scattered and irregular cell activation. Histogram of p-MLC mean intensity
716 frequency (n=4 of each genotype) demonstrate higher scattering of staining in *Myh11:Cre*$^{ERT2}$*;*
717 *Lox*$^{fl/fl}$ mutant aortas than in the control (*Myh11:Cre*$^{ERT2}$) (F). Dotted lines indicate median values.

718

719

720

721 **Supplementary Figures**

722 **Supplementary Figure 1. SMC-specific Lox deletion following hypertension leads to aneurysm**
723 **formation.** Western blot (A) and quantification (B) for Lox from aortas of control (*Lox*$^{fl/fl}$) or
724 Mutant (*Myh11:Cre*$^{ERT2}$*; Lox*$^{fl/fl}$ or *Myh11:Cre*$^{ERT2}$*; Lox*$^{\Delta/fl}$) with no AngII infusion.

725 **Supplementary Figure 2. *LOX* knockdown in HAOSMC affects multiple processes.** Western blot
726 for LOX from HAOSMC lysates treated with LOX inhibitors (A). HAOSMCs treated with LOX
727 inhibitors do not show a significant size difference. Immunostaining of *shCtrl* and *shLOX* HAOSMCs
728 for Ki-67 (C). Red staining indicate Ki-67 positive cells. Quantification of Ki-67 positive cells (D).
729 Live cell imaging markers of cell proliferation (E) and cell death (F) of *shCtrl* and *shLOX* HAOSMC
730 show reduced proliferation and augmented cell death in *shLOX* cells. Confocal images of DAPI
731 nuclei staining and their Imaris 3D models (G). Quantification of regular disc-like nuclei and
732 amorphic nuclei shows an increase of the latter in *shLOX* cells (H).

733 **Supplementary Figure 3. HAOSMC secrete significant LOX and ECM.** Representative ECM protein
734 fold changes between ECM secreted by *shCtrl* and *shLOX* cells (A). HAOSMCs cultured on plastic
735 in high confluency elongate and form layers of cells with a distinct direction (B). Following removal
736 of the cells, ECM directionality can still be observed (C). Black arrows indicate the ECM
737 directionality. Western blot for LOX from HAOSMC conditioned media showing LOX is highly
738 secreted from the cells (D). Three independent conditioned media are shown. Quantification of
739 *shCtrl* and *shLOX* average cell area following their co-seeding with parental HAOSMCs (E).

740 **Supplementary Figure 4. LOX is physically associated with cytoskeletal proteins**. KEGG (A) and
741 IPA (B) analyses of proteins immunoprecipitated with LOX and identified by LC-MS/MS show
742 enrichment of cytoskeletal proteins. Cytoskeletal-associated clusters are highlighted.

743 **Supplementary Figure 5. Hypertension is required for inducing aneurysms following *Lox***
744 **deletion in SMC.** Male and female mice of the indicated genotypes following AngII infusion for 28
745 days develop multiple aneurysms throughout the aorta length.

746 **Supplementary Figure 6. Abnormal mitochondrial appearance in *Lox* mutant medial SMC.**
747 Mitochondrial area (A), major axis (B) and eccentricity (C) were monitored in control
748 *Myh11:Cre*$^{EGFP}$ and mutant *Myh11:Cre*$^{EGFP}$*; Lox*$^{fl/fl}$ medial SMC. Significant differences were
749 observed in the shape of the mitochondria but not their area between the two genotypes. n= 4
750 mice of each genotype.